

Highlights

A general representation of the Leader-based Connected Automated Vehicle platoon and stability analyses considering multiple delays

Tiancheng Ruan,Hao Wang,Xiaopeng Li,Yujia Chen,Changyin Dong

- A novel and more unconservative stability condition of the CAV platoon is derived under the general representation proposed based on the Lyapunov-Krasovskii Stability Theorem.
- The Bessel-Legendre inequalities are employing to obtain less conservative stability condition.
- A comprehensive performance evaluation analysis of different control parameters and four typical Leader-based IFTs is performed to reveal tracking performance, transient response, and safety conditions in a variety of scenarios.

A general representation of the Leader-based Connected Automated Vehicle platoon and stability analyses considering multiple delays

Tiancheng Ruan^{a,b,c}, Hao Wang^{a,b,c,*}, Xiaopeng Li^d, Yujia Chen^{a,b,c} and Changyin Dong^{a,b,c}

^aJiangsu Key Laboratory of Urban ITS, Southeast University, 2 Si Pai Lou, Nanjing, 210096, P.R. China

^bJiangsu Province Collaborative Innovation Center of Modern Urban Traffic Technologies, 2 Si Pai Lou, Nanjing, 210096, P.R. China

^cSchool of Transportation, Southeast University, 2 Si Pai Lou, Nanjing, 210096, P.R. China

^dDepartment of Civil & Environmental Engineering, University of Wisconsin-Madison, 1415 Engineering Drive, Madison, 53706, USA

ARTICLE INFO

Keywords:

Connected Automated Vehicle (CAV)
CAV platoon
General modeling of CAV platoon
Stability analyses
State delay system

ABSTRACT

Urged by the potential of Connected Automated Vehicles (CAVs), research has recently focused on studying their benefits on safety, emissions, and capacity. However, achieving these benefits is contingent on ensuring stability, which is the fundamental objective of CAVs. Despite the common employment of feedback control to attain stability, it cannot be guaranteed with certainty due to the inherent communication delay present in CAVs. Therefore, this paper proposes a general representation of the Leader-based CAV platoon considering multiple delays. Moreover, a novel stability condition of the CAV platoon is derived under the general representation proposed based on the Lyapunov-Krasovskii Stability Theorem and Bessel-Legendre inequalities. In addition, a thorough numerical analysis is conducted in diverse scenarios to comprehensively evaluate the tracking performance and safety conditions of various control parameters and information flow topologies (IFTs). The results show that the CAV platoon has superior tracking performance in various scenarios if stability is guaranteed. Moreover, increasing the gain of the velocity error within a suitable range can moderately improve tracking performance and safety condition. Furthermore, receiving more information in most cases enables smoother tracking process.

1. Introduction

Over a century since the advent of the automobile, the goal of providing safer and more comfortable transportation services has been a persistent commitment of automotive engineers. Despite advances in technology, traffic issues such as congestion, accidents, and pollution have become increasingly prominent in recent decades (Schrank et al., 2012; Jin and Orosz, 2016). Traditional traffic engineering approaches, including traffic management and control, have been used to improve traffic capacity and service levels. However, these methods are gradually facing bottlenecks in addressing the ever-growing demand for transportation. A study of the dynamic and static characteristics of traffic flow has identified the main cause to be the significant heterogeneity of human factors, which leads to uncertainty in road traffic (Zhong et al., 2020; Ye and Yamamoto, 2018; van Arem et al., 2016; Yu et al., 2021), further deteriorating traffic flow stability and restricting capacity.

Automated Vehicles (AVs) are emerging as a promising solution and have gained significant attention from both academia and the automotive industry in recent years. By using on-board sensory devices, AVs track their predecessor to maintain a constant gap or time gap. The availability of AVs as standard equipment in modern commercial vehicles is increasing, resulting in a rising market penetration rate (Wilson and Ward, 2011). Despite their relatively short history, extensive research has demonstrated their benefits in terms of safety, emissions, and capacity compared to human drivers (Wang et al., 2019; Sarker et al., 2019; Dey et al., 2015).

However, AV is inadequate to fully liberate the potential of autonomous driving since information only acquired by on-board sensors. Thanks to the development of Cellular vehicle-to-everything (C-V2X) and wireless communication technology, Connected Automated Vehicle (CAV) emerges by using Vehicle-to-Infrastructure (V2I) / Vehicle-to-Vehicle (V2V) communication to further improve safety and capacity. CAV has the potential to achieve more complex controls compared to AV due to its ability to obtain more adequate and timely information through communication (Navas and Milanés, 2019; Ruan et al., 2021; Zhou et al., 2021). Currently, there has been abundant research on CAVs,

*Corresponding author

 ruantiancheng@seu.edu.cn (T. Ruan); haowang@seu.edu.cn (H. Wang); xli2485@wisc.edu (X. Li); chenyujia@seu.edu.cn (Y. Chen); dongcy@seu.edu.cn (C. Dong)

ORCID(s):

including exploring its gain in capacity (Ghiasi et al., 2017; Chang et al., 2020), stability (Zhou et al., 2019; Montanino and Punzo, 2021), eco-driving (Qin et al., 2018; Ruan et al., 2022), and the design of control strategies of CAVs (Zhu et al., 2019; Chen et al., 2021).

Despite the advantages of CAVs mentioned above, these benefits are based on the premise of achieving the fundamental goal of stability, which means that transient responses induced by disturbances will gradually decay over time. Past research has employed closed-loop feedback control to ensure the stability of CAVs (Eyre et al., 1998; Will and Z AK, 1997). However, the effectiveness of closed-loop feedback control is questionable due to the unavoidable existence of communication delays (Abdallah et al., 2011). Specifically, communication delays can result in alterations to the timing of a system's response, known as phase shifts. When addressing this challenge, employing feedback control to stabilize the system with time delays may encounter issues. The stability domain could shrink, and the risk of overcompensation might increase. Overcompensation denotes a scenario in which the system's corrective actions are excessively forceful, causing undesirable oscillations or instability rather than attaining the desired stability. Therefore, extensive research has been conducted to derive stability conditions that consider time delays (Wang et al., 2018a; Hua et al., 2022; Wang et al., 2022).

In spite of the wide array of methods utilized in current research, they can generally be classified into two primary groups: frequency-domain methods and time-domain methods. In earlier research, stability conditions were primarily derived using frequency-domain methods (Chandler et al., 1958; Li et al., 2019). Herman et al. (Herman et al., 1959; Gazis et al., 1963) enhanced this approach by using a Laplace transform-based technique to derive characteristic equations for a linear time-delay model and obtaining stability conditions through numerical methods. Zhang and Jarrett (Zhang and Jarrett, 1997; Jarrett and Xiaoyan, 1993) further refined this approach by incorporating sensitivity and reaction time in a linear time-delay model and using a characteristic equation-based approach to derive a more comprehensive and analytical stability condition. Kamath et al. (Kamath et al., 2015) employed a similar approach to derive stability conditions for the optimal velocity model and the classical car-following model under reaction delay, utilizing the Nyquist stability criterion to construct the characteristic equation. Despite the effectiveness of frequency-domain methods in deriving stability conditions considering delays, there are still significant limitations that need to be addressed. Concretely, in frequency-domain methods, the communication delay is incorporated in the term $e^{-j\omega\tau}$, where ω represents the angular frequency and τ denotes the communication delay. The frequency-dependent phase shift caused by the delay term leads to a continuous change in phase across the entire frequency spectrum, resulting in the delay term exhibiting high dimensionality. This high dimensionality of the delay term turns the stability condition derivation into an infinite-dimensional problem, hindering frequency-domain methods from analytically deriving stability conditions. Consequently, the Fourier form $e^{ix} = \cos x + i \sin x$ or Euler's formula $f(x) = f(a) + \dot{f}(a)(x - a) + \frac{\ddot{f}(a)}{2!}(x - a)^2 + \dots$ are employed to linearize functional differential equations into ordinary differential equations (Lhachemi and Prieur, 2020). Although such linearization enables frequency-domain methods to derive stability conditions considering delays, it introduces approximations, leading to inaccuracies and reduced precision.

Alternatively, time-domain methods, primarily the Second Lyapunov method, have exhibited superiority in stability analyses considering delays. Utilizing state-space representation, communication delays are incorporated into time-delayed states and are solved by leveraging advanced mathematical tools, such as the Linear Matrix Inequality approach. For instance, Li et al. (Li et al., 2016; Wu et al., 2018) utilized the Second Lyapunov method and LaSalle's invariance principle to derive stability conditions for CAVs using feedback-based control under time delays, and conducted simulations to evaluate the impact of time delays on tracking performance. Gao et al. (Gao et al., 2016) constructed a third-order state-space equation representing CAV platoon state dynamics considering delays and derived the corresponding stability conditions represented as delay-dependent linear matrix inequality. Subsequently, Sun et al. (Sun et al., 2018) conducted a comprehensive review of these methods and verified the consistency and applicability of some stability conditions through numerical simulations. However, time delays introduce a dependency on the past states of the system, which cannot be represented as finite-dimensional state vectors. This dependency on past states introduces an infinite-dimensional aspect to the problem, necessitating the extension of the Second Lyapunov method to the functional space for solving stability conditions considering delays. During this extension process, an additional constraint is added that the Lyapunov functional must hold along all system trajectories (Fridman, 2006, 2014; Wang et al., 2016; Lian et al., 2020). Therefore, a stability analysis method that can handle delays without introducing additional constraints needs to be developed to obtain more accurate stability conditions.

To address the gap in the literature, this paper introduces a general supermatrix representation of the leader-based CAV platoon that accounts for communication delay and engine actuator delay. Furthermore, to derive stability

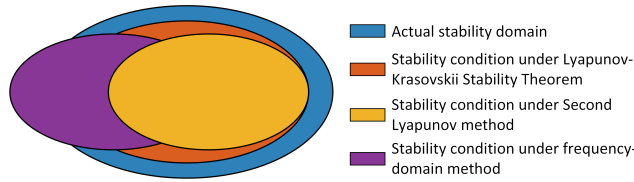


Figure 1: The schematic of the relationship between the actual stability domain and the stability conditions derived from frequency-domain methods, the Second Lyapunov Method, and the Lyapunov-Krasovskii Stability Theorem.

conditions, the Lyapunov-Krasovskii Stability Theorem is employed, which is one of the extensions of the Second Lyapunov method in the functional space. Unlike the Second Lyapunov method, the Lyapunov-Krasovskii Stability Theorem only requires the Lyapunov-Krasovskii Functional mapping in the Banach space holds along the system trajectory, rather than along all system trajectories. Furthermore, the objective of methodological development in stability analysis is to obtain stability conditions that more closely align with the actual stability domain. Therefore, the stability conditions derived from frequency-domain methods, the Second Lyapunov method, and the Lyapunov-Krasovskii Stability Theorem are depicted in Fig. 1 to illustrate their relationship with the actual stability domain. It is important to note that the stability domains in the figure only represent containment relationships, and their areas have no practical meaning. The stability conditions obtained from the Second Lyapunov method are entirely encompassed by the stability conditions derived from the Lyapunov-Krasovskii Stability Theorem, as the latter removes unnecessary constraints in its methodology and provides more accurate stability conditions. The analytical relationship between them is discussed in detail in Appendix E. Regarding frequency-domain methods, although there is no direct containment relationship between the stability conditions derived from them and those obtained from time-domain methods, such as Lyapunov-based methods, frequency-domain methods resort to linear approximations to solve for stability conditions considering delays, resulting in inaccuracies and sometimes exceeding the actual stability domain, while time-domain methods provide sufficient conditions that are included in the actual stability domain. Moreover, utilizing the properties of Bessel-Legendre inequalities enables deriving more accurate stability conditions compared to traditional integral inequalities. Additionally, extensive numerical analyses are conducted in various scenarios to comprehensively evaluate the tracking performance and safety conditions of different control parameters and provide guidance for their selection. In summary, contributions of this paper can be divided into three parts:

1. The derivation of a novel and accurate stability condition of the CAV platoon considering multiple delays based on the Lyapunov-Krasovskii Stability Theorem.
2. The utilization of the Bessel-Legendre inequalities to obtain a more accurate stability condition.
3. Extensive numerical analyses are conducted in various scenarios to comprehensively evaluate the tracking performance and safety conditions of different control parameters and provide guidance for their selection.

The remainder of the paper is outlined as follows: Section 2 presents the modeling of the general representation of the Leader-based CAV platoon. Corresponding stability analyses and the derivation of stability conditions based on the Lyapunov-Krasovskii Stability Theorem are carried out in Section 3. Section 4 proposes a comprehensive performance evaluation analysis of different control parameters. We summarize the paper in Section 5.

Notation throughout the paper:

\mathbb{R}^n denotes the n-dimensional Euclidean space with Euclidian norm $|\cdot|$.

$\mathbb{R}^{m \times n}$ deontes the set of all $m \times n$ real matrices.

\mathbb{S}_n means the set of symmetric matrices of $\mathbb{R}^{n \times n}$.

\mathbb{S}_n^+ denotes the set of symmetric positive definite matrices.

A^T stands for the transpose of a vector or a matrix A .

The symmetric matrix $\begin{bmatrix} A & B \\ * & C \end{bmatrix}$ denotes $\begin{bmatrix} A & B \\ B^T & C \end{bmatrix}$.

$He(K)$ represents $K + K^T$ for any square matrix $K \in \mathbb{R}^{n \times n}$.

I_n defines the identity matrix of $n \times n$.

$0_{m,n}$ denotes the zero matrix of $m \times n$ dimension.

For any matrix $A \in \mathbb{R}^{n \times n}$, $A > 0$ denotes that A is symmetric and positive definite.

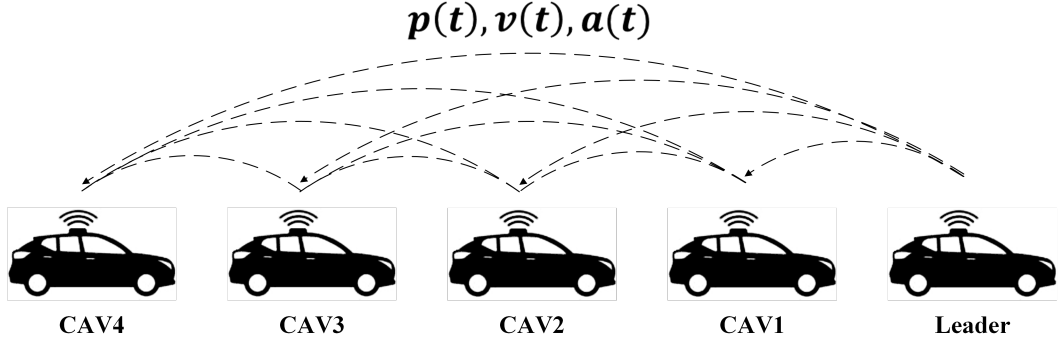


Figure 2: The schematic of the CAV platoon.

The Banach space $C([-h, 0], \mathbb{R}^n)$ refers to the set of continuous functions from the interval $[-h, 0] \subset \mathbb{R}$ to \mathbb{R}^n that are square integrable.

For any function $f \in C$, the uniform norm $|f|_h$ refers to $\sup_{\theta \in [-h, 0]} |f(\theta)|$.

$\text{diag}\{a_1, a_2, \dots, a_n\}$ stands for the diagonal matrix $\begin{bmatrix} a_1 & 0 & 0 \\ 0 & \ddots & 0 \\ 0 & 0 & a_n \end{bmatrix}$ whose diagonal elements from the top left corner are a_1, a_2, \dots, a_n .

Let $A \in \mathbb{R}^{m \times n}$ and $B \in \mathbb{R}^{p \times q}$. The Kronecker product of A and B is denoted as $A \otimes B$ and defined as follows:

$$A \otimes B = \begin{bmatrix} a_{11}B & \cdots & a_{1n}B \\ \vdots & \ddots & \vdots \\ a_{m1}B & \cdots & a_{mn}B \end{bmatrix} \in \mathbb{R}^{mp \times nq}.$$

Let $C \in \mathbb{R}^{m \times n}$ and $D \in \mathbb{R}^{m \times n}$. The Hadamard product of C and D is denoted as $C \circ D$ and defined as follows:

$$C \circ D = \begin{bmatrix} c_{11}d_{11} & \cdots & c_{1n}d_{1n} \\ \vdots & \ddots & \vdots \\ c_{m1}d_{m1} & \cdots & c_{mn}d_{mn} \end{bmatrix} \in \mathbb{R}^{m \times n}.$$

2. CAV platoon modeling

In this scenario, a platoon of n CAVs is considered to be moving along a single lane, and the schematic of this CAV platoon is illustrated in Fig. 2, where the dashed line indicates communication between two CAVs. The platoon of CAVs can be modeled as a weighted directed graph (digraph) $\mathcal{G} = \{\mathcal{V}, \mathcal{E}, \mathcal{A}\}$, where each vehicle in the platoon is represented as a node, and intervehicle communication is represented as an edge. The set of nodes \mathcal{V} is defined as $\{1, 2, \dots, n\}$, and the set of edges \mathcal{E} is a subset of $\mathcal{V} \times \mathcal{V}$. The weighted adjacent matrix $\mathcal{A} = [a_{ij}]n \times n$ with nonnegative elements represents the communication links between nodes, where $a_{ii} = 0$ indicates that self-edges (i, i) are not allowed unless specified otherwise. The weight a_{ij} represents the communication strength from node i to node j . The degree matrix of \mathcal{G} is defined as $\mathcal{D} = \text{diag}\{d_1, d_2, \dots, d_n\}$, where $d_i = \sum_{j \in \mathcal{V}} a_{ij}$. Within the time duration, the longitudinal

position, speed, acceleration, and jerk of vehicle $i \in \mathcal{V}$ at time t are denoted as $p_i(t)$, $v_i(t) = \dot{p}_i(t)$, $a_i(t) = \ddot{p}_i(t)$, and $\dot{a}_i(t) = \ddot{p}_i(t) \in \mathbb{R}$, respectively. Although each CAV communicates with all other CAVs in the platoon arbitrarily for generalization purposes in the schematic, the communication digraph varies in practice, based on the IFT adopted. Via intra-vehicle communication (e.g., C-V2X according to the meeting report from Federal Communications Commission (Verizon North, 2020)), all vehicles share their state information (e.g., the absolute position, velocity, and acceleration) with other vehicles within the platoon according to the IFT. An assumption made is that each CAV is fitted with the following components: (i) an on-board radar for detecting potential collisions by measuring the gap distance between consecutive vehicles, (ii) a GPS sensor for obtaining the longitudinal position, (iii) a wireless on-board unit that allows

communication of relevant information with proximal vehicles via C-V2X communication (Verizon North, 2020), (iv) an upper-level controller that calculates the desired longitudinal acceleration based on the obtained parameters, and (v) a lower-level controller that determines the throttle and brake actuator inputs to follow the desired acceleration (Milanés et al., 2013). The aforementioned assumption is deemed reasonable since the required sensing, communication, and actuation units are already available in contemporary CAVs, and no alterations to the current vehicle configuration are needed. It is worth mentioning that the on-board radar only serves as a validation check unless in the event of communication unavailability or failure, as communication is a more efficient means of acquiring more accurate information.

2.1. Vehicle longitudinal dynamic Modeling

The longitudinal dynamics of a vehicle can be modeled by a complex system consisting of several components, including the engine, throttle and brake actuators, drive train, transmission, and torque converter. When subjected to various resistance forces, the longitudinal dynamic of vehicle i can be described by a force balance equation:

$$m_i a_i(t) = f_i^e(t) - f_i^g(t) - f_i^w(t) - f_i^r(t) \quad (1)$$

where m_i stands for the unknown mass of vehicle i ; $f_i^e(t)$ is the desired engine force acting on vehicle i ; $f_i^g(t)$, $f_i^w(t)$, and $f_i^r(t)$ denote the gravity component parallel to the road surface, air resistance force, and rolling resistance force, respectively.

However, due to the nonlinearity of Equation (1), designing a suitable controller is challenging. Therefore, a feedback control approach discussed in Appendix B is utilized to transform Equation (1) into a linear form (Wang, 2018):

$$\tau_i \dot{a}_i(t) + a_i(t) = u_i(t) \quad (2)$$

where $u_i(t)$ denotes the control input of the lower-level controller, which can be interpreted as the desired acceleration of vehicle i , τ_i is the time constant representing the engine actuator delay.

Reformulate Equation (2), the state space equation can be represented as:

$$\dot{x}_i(t) = Ax_i(t) + Bu_i(t) \quad (3)$$

$$\text{with } A = \begin{bmatrix} 0 & 1 & 0 \\ 0 & 0 & 1 \\ 0 & 0 & -\frac{1}{\tau_i} \end{bmatrix} \text{ and } B = \begin{bmatrix} 0 \\ 0 \\ \frac{1}{\tau_i} \end{bmatrix}$$

where $x_i(t) = [p_i(t) \ v_i(t) \ a_i(t)]^T \in \mathbb{R}^3$ denotes the state vector of vehicle i .

As for the reference leading dynamics, it can be described as (Hengster-Movric et al., 2015):

$$\dot{x}_1(t) = Ax_1(t) \quad (4)$$

where $x_1(t) = [p_1(t) \ v_1(t) \ a_1(t)]^T \in \mathbb{R}^3$.

An appropriate decentralized coupling protocol of communication information is used to determine the control input of vehicle i due to the presence of limited communication in the control strategy:

$$u_i = u_i \underbrace{\left(x_1(t-h), \dots, x_i(t-h), \dots, x_n(t-h) \right)}_n \quad (5)$$

where h represents the communication delay within the transmission range which is assumed to be similar among different IFTs (Zheng et al., 2015; Vukadinovic et al., 2018; Vu et al., 2020; Martín-Sacristán et al., 2020; Pirani et al., 2022).

Assuming that CAVs adopt the Constant Distance (CD) policy and Leader-based IFT, which involves maintaining a desired distance from the reference leader, the cooperative leader tracking problem can be formulated as follows (Wang et al., 2018b):

$$\begin{cases} \lim_{t \rightarrow \infty} \|p_i(t) - p_1(t) - d_{i1}\| = 0 \\ \lim_{t \rightarrow \infty} \|v_i(t) - v_1(t)\| = 0 \quad \forall i = 1, \dots, N \\ \lim_{t \rightarrow \infty} \|a_i(t) - a_1(t)\| = 0 \end{cases} \quad (6)$$

where d_{i1} denotes the desired intra-vehicle distance of vehicle i from the leading vehicle.

The decentralized coupling protocol computed onboard by vehicle i to adjust its dynamics and achieve the consensus goal (6) is as follows:

$$u_i = - \sum_{j=1}^n a_{ij} k_{ij}^T [p_i(t-h) - p_j(t-h) - d_{ij} \quad v_i(t-h) - v_j(t-h) \quad a_i(t-h) - a_j(t-h)]^T \quad (7)$$

where

a_{ij} denotes the weight of the edge (i, j) , and $a_{ij} = 0$ if there is no edge (i, j) ;

d_{ij} stands for the desired intra-vehicle distance of vehicle i from the vehicle j ;

$k_{ij} = [\alpha_{ij} \quad \beta_{ij} \quad \gamma_{ij}]^T \in \mathbb{R}^3$ presents the feedback control gain vector;

α_{ij}, β_{ij} , and γ_{ij} denote the control gain of spacing error, speed error, and acceleration error, respectively.

2.2. Closed-loop Vehicle Network Modeling

To establish the consensus of systems (3) and (4) under the influence of the coupling protocol (7), the error state is defined with respect to the leader as follows:

$$e_i(t) = \begin{bmatrix} \tilde{p}_i \\ \tilde{v}_i \\ \tilde{a}_i \end{bmatrix} = \begin{bmatrix} p_i - p_1 - d_{i1} \\ v_i - v_1 \\ a_i - a_1 \end{bmatrix} \quad (8)$$

Then the decentralized coupling protocol (7) can be reformulated as:

$$u_i = - \sum_{j=1}^n a_{ij} k_{ij}^T [e_i(t-h) - e_j(t-h)] \quad (9)$$

Therefore, the dynamics of the error system can be presented as:

$$\begin{cases} \dot{\tilde{p}}_i = \tilde{v}_i \\ \dot{\tilde{v}}_i = \tilde{a}_i \\ \dot{\tilde{a}}_i = -\frac{1}{\tau} \tilde{a}_i - \frac{1}{\tau} \sum_{j=0}^n a_{ij} k_{ij}^T (e_i(t-h) - e_j(t-h)) \end{cases} \quad (10)$$

From Equation (10), the dynamics of the closed-loop vehicular network can be recast in a compact form as:

$$\dot{e}_i(t) = A e_i(t) - B \sum_{j=0}^n a_{ij} k_{ij}^T (e_i(t-h) - e_j(t-h)) \quad (11)$$

Theorem 1 *The closed-loop network system adopting constant communication delay, Leader-based IFT, and CD policy can be presented as a linear state delay system:*

$$\begin{cases} \dot{X}(t) = A^* X(t) + \Psi X(t-h), & \forall t \geq 0 \\ X(t) = \phi(t), & \forall t \in [-h, 0] \end{cases} \quad (12)$$

with

$$\left\{ \begin{array}{l} A^* = I_n \otimes A \in \mathbb{R}^{3n \times 3n} \\ \Psi = -B^* \mathcal{F} (E_1 - E_2) \in \mathbb{R}^{3n \times 3n} \\ B^* = I_n \otimes B \in \mathbb{R}^{3n \times n} \\ \mathcal{K} = [k_{ij}^T]_{n \times n} \\ \mathcal{H} = \mathcal{A}^\circ \mathcal{K} = [a_{ij} \otimes k_{ij}^T]_{N \times N} \in \mathbb{R}^{n \times 3n} \\ \mathcal{F} = \text{diag} \underbrace{\{\mathcal{H}_1, \mathcal{H}_2, \dots, \mathcal{H}_N\}}_n \in \mathbb{R}^{n \times 3n^2} \\ \mathcal{H}_i = \underbrace{[a_{i1} k_{i1}^T, a_{i2} k_{i2}^T, \dots, a_{in} k_{in}^T]}_n \in \mathbb{R}^{1 \times 3n} \forall i \in \mathcal{V} \\ E_1 = \text{diag} \underbrace{\{I_1, I_1, \dots, I_1\}}_n \in \mathbb{R}^{3n^2 \times 3n} \\ E_2 = \underbrace{[I_2^T \ \dots \ I_2^T]}_n {}^T \in \mathbb{R}^{3n^2 \times 3n} \\ I_1 = \underbrace{[I_3^T \ \dots \ I_3^T]}_n {}^T \in \mathbb{R}^{3n \times 3} \\ I_2 = I_{3n} \in \mathbb{R}^{3n \times 3n} \\ I_3 = I_3 \in \mathbb{R}^{3 \times 3} \end{array} \right.$$

where $X(t) = [e_1^T \ \dots \ e_n^T]^T \in \mathbb{R}^{3n}$ stands for the error state vector of the closed-loop vehicular network; ϕ is the initial conditions; A^* and Ψ are constant matrix according to their definitions.

Proof **Theorem 1** can be obtained by manipulating matrix transformations on the error state vector of the closed-loop vehicular network and Equation (11).

3. Stability analyses

Before delving into the analyses, we first introduce some fundamental mathematical preliminaries that will be employed in subsequent analyses.

The Lyapunov-Krasovskii Stability Theorem is a widely used method for stability analysis of state delay systems. This approach extends the Second Lyapunov method to functional space and involves the use of "energy" functionals that are positive definite and decrease along the system's trajectories (Gu et al., 2003). The Lyapunov-Krasovskii theorem is presented below:

Lemma 2 (Lyapunov-Krasovskii Stability Theorem (Gu and Liu, 2009)). Given system (12), suppose that f maps $\mathbb{R} \times (\text{bounded sets in } \mathbb{R}^n \times C)$ into bounded sets in \mathbb{R}^n , and that $u, v, w : \mathbb{R}_+ \rightarrow \mathbb{R}_+$ are continuous nondecreasing functions, where additionally $u(s)$ and $v(s)$ are positive for $s > 0$, and $u(0) = v(0) = 0$. If there exists a functional $V : \mathbb{R} \times \mathbb{R}^n \times C \rightarrow \mathbb{R}$ such that

$$\begin{cases} u(|\phi(0)|) \leq V(t, \phi) \leq v(|\phi|_h) \\ \dot{V}(t, \phi) \leq -w(|\phi(0)|) \end{cases} \quad (13)$$

Then the trivial solution of the system (12) is uniformly stable. If $w(s) > 0$ for $s > 0$, then it is uniformly asymptotically stable. If, in addition, $\lim_{s \rightarrow \infty} u(s) = +\infty$, then it is globally uniformly asymptotically stable. Such a functional V is called a Lyapunov-Krasovskii functional (LKF).

Definition 3 (Legendre polynomials (Dattoli et al., 2001)). The Legendre polynomials considered over the interval $[-h, 0]$ are defined by:

$$\mathcal{L}_k(u) = (-1)^k \sum_{l=0}^K p_l^k \left(\frac{u+h}{h} \right)^l, \quad \forall k \in \mathbb{N} \quad (14)$$

where $p_l^k = (-1)^l \begin{pmatrix} k \\ l \end{pmatrix} \begin{pmatrix} k+l \\ l \end{pmatrix}$.

These Legendre polynomials satisfy the following properties (Bos et al., 2017):

Property 4 *P3.1 Orthogonality:*

$$\int_{-h}^0 \mathcal{L}_k(u) \mathcal{L}_l(u) du = \begin{cases} 0, & k \neq l \\ \frac{h}{2k+1}, & k = l \end{cases} \quad \forall (k, l) \in \mathbb{N}^2 \quad (15)$$

P3.2 Boundary conditions:

$$\begin{cases} \mathcal{L}_k(0) = 1, \\ \mathcal{L}_k(-h) = (-1)^k, \end{cases} \quad \forall k \in \mathbb{N}, \quad (16)$$

P3.3 Differentiation:

$$\dot{\mathcal{L}}_k(u) = \begin{cases} 0, & k = 0 \\ \sum_{i=0}^{k-1} \frac{(2i+1)}{h} (1 - (-1)^{k+i}) \mathcal{L}_i(u), & k \geq 1 \end{cases} \quad (17)$$

We remark that the set of Legendre polynomials $\{\mathcal{L}_k, k \in \mathbb{N}\}$ forms an orthogonal sequence according to the *P3.1 Orthogonality*.

Definition 5 (*Bessel inequality (Dragomir, 2001)*). Given $\{\mathcal{L}_k, k \in \mathbb{N}\}$ be an orthogonal sequence, for any scalar function $\phi : [-h, 0] \rightarrow \mathbb{R}$, the following inequality holds:

$$\langle \phi, \phi \rangle \geq \sum_{k=0}^N \frac{\langle \phi, \mathcal{L}_k \rangle^2}{\langle \mathcal{L}_k, \mathcal{L}_k \rangle} \quad (18)$$

Lemma 6 (*Bessel-Legendre inequalities (Lee et al., 2018)*). Assuming $x \in C$, $R \in \mathbb{S}_n^+$, and $h > 0$, the following inequality holds:

$$\int_{-h}^0 x^T(u) Rx(u) du \geq \frac{1}{h} \begin{bmatrix} \Omega_0(x) \\ \Omega_1(x) \\ \vdots \\ \Omega_N(x) \end{bmatrix}^T R_N \begin{bmatrix} \Omega_0(x) \\ \Omega_1(x) \\ \vdots \\ \Omega_N(x) \end{bmatrix} \quad (19)$$

where $\Omega_k(x) = \int_{-h}^0 \mathcal{L}_k(u) x(u) du$, $k = 0, \dots, N$ and $R_N = \text{diag}\{R, 3R, \dots, (2N+1)R\}$.

Proof See Appendix A for detailed proof.

Remark 7 The Bessel-Legendre inequalities have specific cases where $N = 0$ and $N = 1$, which have been shown to correspond to other well-known inequalities such as Jensen's Inequality, the Wirtinger-based integral inequality, and the auxiliary function-based integral inequality in previous research (Seuret and Gouaisbaut, 2013; Park et al., 2015).

Remark 8 The basis of $C([-h, 0], \mathbb{R}^n)$ can be represented by the orthogonal set of sequences $\{\mathcal{L}_k, k \in \mathbb{N}\}$, which is dense in $C([-h, 0], \mathbb{R}^n)$. Moreover, the Bessel-Legendre inequality approaches equality when the value of N tends to ∞ :

$$\int_{-h}^0 x^T(u) Rx(u) du = \frac{1}{h} \begin{bmatrix} \Omega_0(x) \\ \Omega_1(x) \\ \vdots \\ \Omega_N(x) \end{bmatrix}^T R_N \begin{bmatrix} \Omega_0(x) \\ \Omega_1(x) \\ \vdots \\ \Omega_N(x) \end{bmatrix} \quad (20)$$

The main concept behind Lemma 2 is to establish a positive definite functional whose derivative with respect to time along the trajectories of system (12) is negative definite. Thus, the local stability of the closed-loop network system (12) can be ensured by proposing a candidate LKF V and establishing certain conditions that guarantee its positive definiteness and the negative definiteness of its derivative. In LKF-based stability analysis of such systems,

various types of functionals have been proposed in the literature, among which an integral quadratic term is a prominent component (Fridman et al., 2003):

$$V(X_t) = \int_{-h}^0 \int_u^0 \dot{X}_t^T(\theta) R \dot{X}_t(\theta) d\theta du \quad (21)$$

Differentiating Equation (21) with respect to t leads to:

$$\dot{V}(X_t) = h \dot{X}_t^T(t) R \dot{X}_t(t) - \int_{-h}^0 \dot{X}_t^T(u) R \dot{X}_t(u) du \quad (22)$$

To convert Equation (22) into a suitable LMI setup, an over-approximation process of the integral terms is adopted since they cannot be directly converted in the quadratic formulation described above.

Thanks to Lemma 6, the lower bound of $\int_{-h}^0 \dot{X}_t^T(u) R \dot{X}_t(u) du$ can be derived by the following Corollary:

Corollary 9 *Let x be such that $\dot{x} \in C$, $R \in \mathbb{S}_n^+$, and $h > 0$. Then, the integral inequality*

$$\int_{-h}^0 \dot{x}^T(u) R \dot{x}(u) du \geq \frac{1}{h} \xi_N^T \left[\sum_{k=0}^N (2k+1) \Gamma_N(k)^T R \Gamma_N(k) \right] \xi_N, \quad (23)$$

holds for all integers $N \in \mathbb{N}$ where

$$\xi_N = \begin{cases} \begin{bmatrix} x^T(0) & x^T(-h) \end{bmatrix}^T, & \text{if } N = 0, \\ \begin{bmatrix} x^T(0) & x^T(-h) & \frac{1}{h} \Omega_0^T & \cdots & \frac{1}{h} \Omega_{N-1}^T \end{bmatrix}^T, & \text{if } N > 0, \end{cases} \quad (24)$$

Proof See Appendix C for detailed proof.

Define the lower bound by Corollary 9, and the stability theorem with an arbitrary N follows.

Theorem 10 *For a given integer N and a constant delay h , assume that there exists a matrix $P_N \in \mathbb{S}_{(N+1)n}$ and two matrices $S, R \in \mathbb{S}_n^+$ such that the LMIs*

$$\Theta_N(h) = \begin{cases} P_N > 0, & \text{if } N = 0 \\ P_N + \frac{1}{h} \text{diag}(0_{nn}, S_{N-1}) > 0, & \text{if } N > 0 \end{cases} \quad (25)$$

$$\Phi_N(h) = \Phi_{N0}(h) - \begin{bmatrix} \Gamma_N(0) \\ \vdots \\ \Gamma_N(N) \end{bmatrix}^T R_N \begin{bmatrix} \Gamma_N(0) \\ \vdots \\ \Gamma_N(N) \end{bmatrix} < 0$$

hold, where

$$\begin{cases} \Phi_{N0}(h) = \text{He}(G_N^T(h) P_N H_N) + \tilde{S}_N + h^2 F_N^T R F_N, \\ \tilde{S}_N = \text{diag}\{S, -S, 0_{Nn}\}, \\ S_N = \text{diag}\{S, 3S, \dots, (2N+1)S\}, \\ F_N = \begin{bmatrix} A^* & \Psi & 0_{n,nN} \end{bmatrix}, \\ G_N(h) = \begin{bmatrix} I & 0_n & 0_{n,nN} \\ 0_{nN,n} & 0_{nN,n} & h I_{nN} \end{bmatrix}, \\ H_N = [F_N^T \quad \Gamma_N^T(0) \quad \Gamma_N^T(1) \dots \Gamma_N^T(N-1)]^T. \end{cases} \quad (26)$$

Then system (12) is asymptotically stable for the constant delay h .

Proof See Appendix D for detailed proof.

Table 1
Network and traffic simulation parameters.

| Parameters | Value |
|---|--------------------------|
| Platoon size n | 5 vehicles |
| Vehicle length L | 5 [m] |
| Engine actuator delay τ_i | 0.2 [s] ¹ |
| Communication delay h | 0.3 [s] ² |
| Weight of edge (i, j) | $a_{ij} = \frac{1}{d_i}$ |
| Desired intra-vehicle distance d_{ij} | 15 [m] ³ |

¹ (Wang et al., 2018a; Zhou et al., 2020)

² (Abbas et al., 2018; Thota et al., 2019)

³ (Razzaghpoor et al., 2021)

Remark 11 By setting $N = 0$ in Theorem 10, we can obtain one of the most widely used delay-dependent stability conditions that utilizes Jensen's inequality and LMI (Gouaisbaut and Peaucelle, 2006). Similarly, selecting $N = 1$ will result in the stability conditions presented by Seuret (Seuret and Gouaisbaut, 2013).

Remark 12 The central concept of the Lyapunov-Krasovskii stability theorem is that it is not imperative to establish the negative definiteness of $V(X(t))$ along all system trajectories. Instead, it is adequate to ensure its negative definiteness for solutions that tend to escape the vicinity of $V(X(t)) \leq c$ of the equilibrium. Appendix E provides a comprehensive theoretical analysis of this concept.

Remark 13 The code for constructing the LMIs in Theorem 10 has been uploaded to GitHub for subsequent research. The corresponding URL is attached in Appendix F for further reference.

4. Numerical analyses

In this section, extensive numerical simulations and analyses on the tracking performance and safety conditions of CAV platoon with different feedback control gains employing the Leader-Predecessor-Follower are conducted to illustrate the main results. In addition, the tracking performances of the CAV platoon employing the other Leader-based IFTs are also investigated.

4.1. Simulation setting

To validate the theoretical results, we refer to a platoon consisting of five CAVs (as depicted in Fig. 2) on a single-lane highway as a representative example. According to the definition of Leader-based IFTs, the leader communicates with all vehicles by broadcasting its information while other vehicles only communicate with their neighbors according to the IFT adopted. The caveat is that although parameters should be selected based on the specific control structure in practical. In order to obtain a simulation result for further analysis, the parameters for both network and traffic simulation are reported in Table 1 for simplicity but without loss of generality. Note that the weighted adjacent matrix is set to $a_{ij} = \frac{1}{d_i}, \forall (i, j) \in \mathcal{E}$ denote that all the information of neighbors is playing an equal role in control decisions (Li et al., 2017).

4.2. Numerical analyses under the LPF

In this subsection, several numerical analyses on tracking performance and safety are conducted. To compare and analyze the tracking performance and safety, we consider the most widely adopted Leader-based IFT, LPF, as an example. As for LPF, all CAVs in the platoon obtain information from both the leader and the immediate predecessor as shown in fig. 3, where dotted lines with an arrow denote the one-direction communication. Moreover, each CAV in the platoon takes the same control parameters that meet the Theorem 10. In addition, in order to investigate the effect of different feedback control gains on tracking performance, the following four feedback control gains are selected:

1. Parameter I: $k_i = [0.3, 0.3, 0.3]^T$;

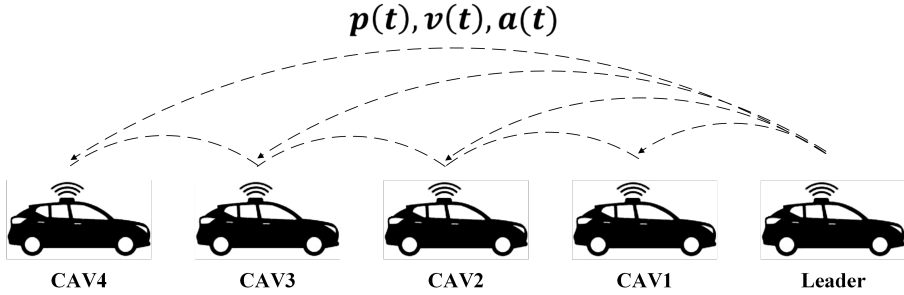


Figure 3: The communication schematic of Leader-Predecessor-Follower (LPF) for the CAV platoon, where dotted lines with an arrow denote the one-direction communication.

2. *Parameter II:* $k_i = [1, 0.3, 0.3]^T$;
3. *Parameter III:* $k_i = [0.3, 1, 0.3]^T$;
4. *Parameter IV:* $k_i = [0.3, 0.3, 1]^T$.

Corresponding matrixes P , S , and R are provided in Appendix F. Moreover, a thorough analysis is carried out on the tracking performance and safety conditions.

4.2.1. Tracking performance analyses

Firstly, in the preliminary analysis, we start considering the tracking performance of CAV platoon employing LPF under different feedback control gains. From this perspective, the tracking performances have been evaluated considering two representative leader maneuvers, namely:

1. **Trapezoidal signal:** The leader suddenly decelerates to $14.6m/s$ at $-0.15m/s^2$ and keeps it for $36s$. Then the leader accelerates back to $20m/s$ at $0.3m/s^2$ (see Fig. 4(a, b)).
2. **Oscillation signal:** The leader suddenly accelerates to $23.6m/s$ in $12s$ and keeps the velocity for $15s$. Then the leader decelerates to $16.4m/s$ in $12s$ and accelerates back to $20m/s$ in $12s$ (see Fig. 4(c, d)).

Once the platoon is formed and all CAVs reach the equilibrium state where the tracking error is 0, we adopt the trapezoidal signal in Fig. 4(a, b) as the leader maneuver to test the tracking performance of the four different feedback control gains under investigation. Results in Fig. 5 confirm the theoretical analysis and show how CAVs track the lead.

As expected, all CAVs in the platoon demonstrate fast and smooth tracking of the leader's motion. Transient changes in the reference signal cause abrupt changes in the tracking error, but these errors diminish over time due to the stability property. Moreover, the tracking speed and overshoot of different CAVs in response to changes in the reference signal are different due to the adoption of different control gains.

Comparing the tracking results under Parameters I and III, it can be found that increasing the gain of the velocity error significantly reduces the number of oscillations and overshoot of the acceleration curve. Additionally, increasing the gain of the spacing error may increase the number of oscillations and overshoot, but it can significantly reduce the tracking error. However, increasing the gain of the acceleration error negatively affects the tracking performance due to drastic fluctuations, even though stability is maintained. Therefore, from the perspective of selecting control parameters, increasing the gain of the velocity error within a suitable range can moderately improve tracking performance.

Furthermore, the tracking performance of the four feedback control gains has been evaluated for the oscillation signal presented in Fig. 4(c, d). Fig. 6 illustrates the tracking performance results, which demonstrates excellent cooperative tracking behavior where each CAV can steadily track the reference signal while maintaining the rigid formation requirements. Additionally, the tracking error, caused by transient changes in the reference signal, decays smoothly over time, similar to the trapezoidal signal. Moreover, as observed in Fig. 5, increasing the gain of the velocity error can effectively improve the tracking performance, while increasing the gain of the acceleration error cannot. Furthermore, Figs. 5 and 6 confirm the effectiveness of the four feedback control gains in tracking performance and stability.

To further investigate the impact of different feedback control gains on tracking performance, three widely used indicators for evaluating transient response, namely Setting Time (ST), Number of Oscillations (NOO), and Maximum

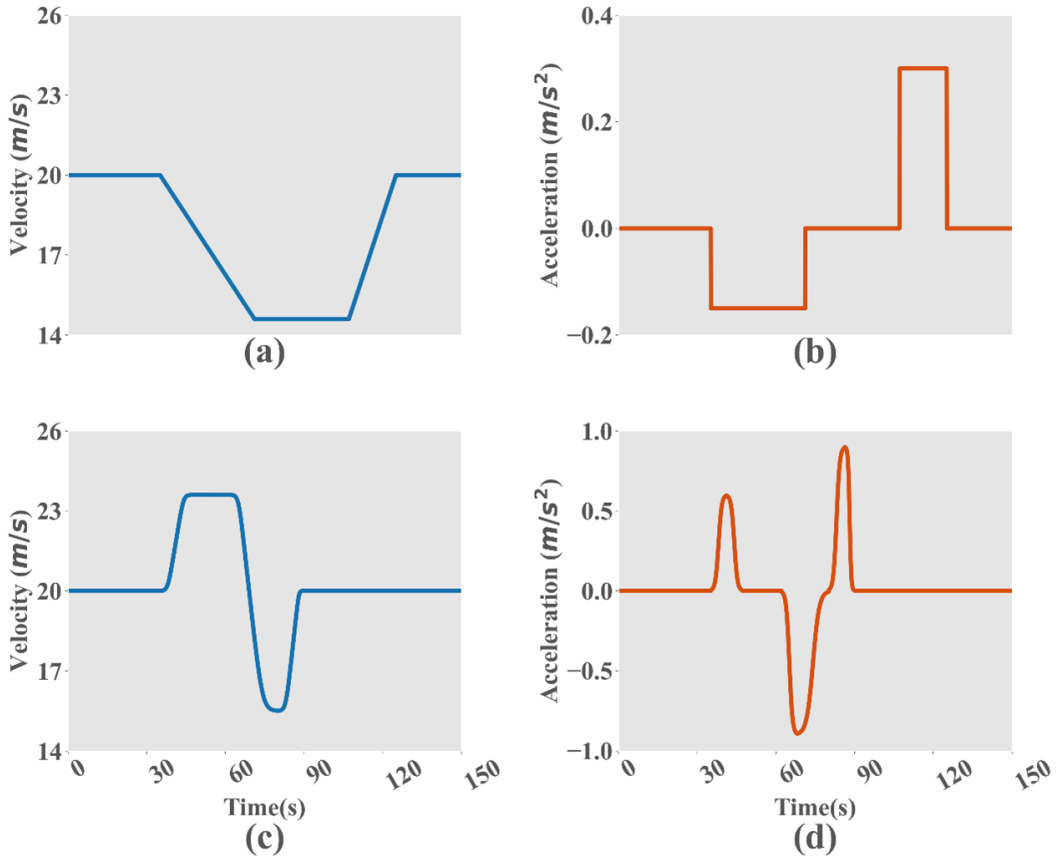


Figure 4: The two representative leader maneuvers: (a) and (b) denote the velocity and acceleration of the trapezoidal signal, respectively; (c) and (d) denote the velocity and acceleration of the oscillation signal, respectively.

Overshoot (MO), have been selected (Ogata, 1995). ST is defined as the time required for the response curve to reach and stay within a certain percentage (2%) of the final value, while NOO represents the number of deviations of the response curve from the final value caused by errors in the setting time. MO, on the other hand, is defined as the maximum peak value of the response curve measured from the desired response of the system. Among these indicators, ST describes the time for the controller to recover from transient response to equilibrium, NOO represents the comfort of the response, and MO denotes the maximum deviation caused by the transient response, reflecting accuracy. As the investigation focuses on the differences in the transient response of different feedback control gains, the leader motion has little impact on the results, and thus only the Trapezoidal signal case is analyzed.

Fig. 7 compares the effects of different feedback control gains on three transient response indicators, namely ST, NOO, and MO. The results indicate that the choice of control gains has a significant impact on the transient response. Specifically, increasing the gain of spacing error, as in Parameter II, leads to smaller MO but larger ST and NOO. On the other hand, increasing the gain of velocity error, as in Parameter III, results in much smaller MO and zero NOO, although ST also increases. Furthermore, increasing the gain of acceleration error, as in Parameter IV, leads to larger ST and NOO, but has almost no effect on MO. It is worth noting that for almost all parameters and indicators, ST, NOO, and MO increase as the vehicle index increases. For Parameter II, although ST also increases as the vehicle index increases, the increase is negligible. Specifically, the ST for Parameter II is 53.8% higher than that of Parameter II for CAV2, but only 5% higher for CAV5. It is worth noting that Parameter III achieves NOO=0, indicating no oscillations during transient response, and thus, exhibits superior safety and comfort performance.

4.2.2. Safety analyses considering hard braking maneuver

To further evaluate the safety in all the different driving and communication scenarios, we have also quantitatively analyzed the possible emergence of critical driving situations for all control gains under investigation by exploiting

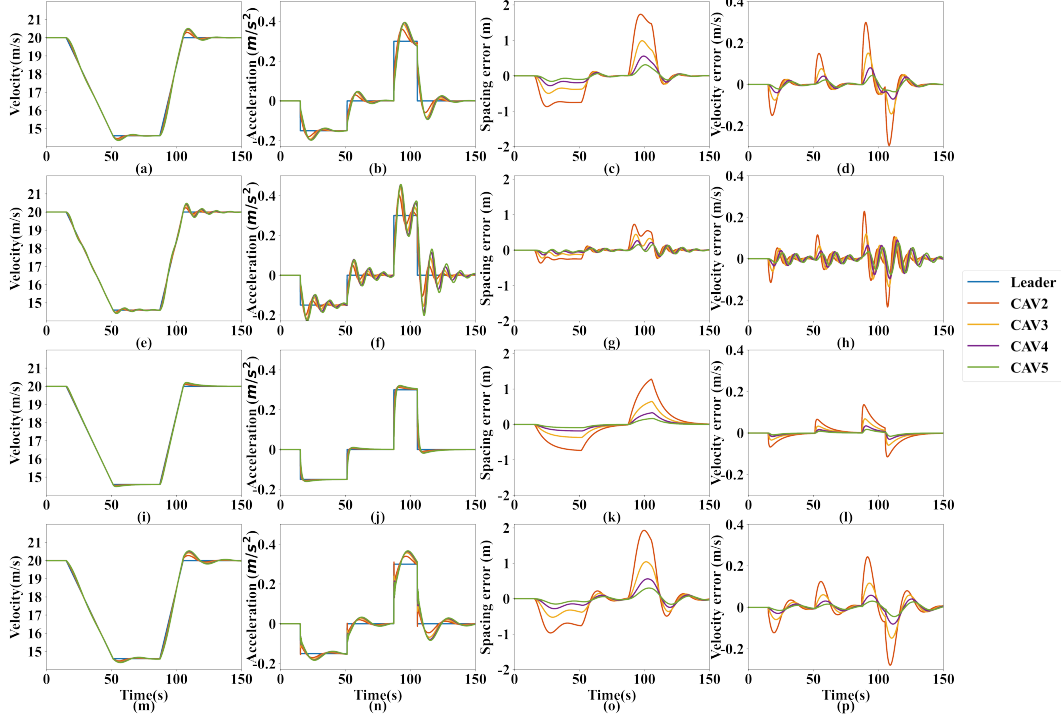


Figure 5: Tracking performance of the CAV platoon for the Trapezoidal signal in Fig. 3(a,b) under the four feedback control gains: (a), (b), (c), and (d) present tracking results under Parameter I, including the velocity, acceleration, tracking error of spacing, and tracking error of velocity, respectively; (e), (f), (g), and (h) show the case under Parameter II; (i), (j), (k), and (l) denote the case under Parameter III; (m), (n), (o), and (p) show the case under Parameter IV.

the safety indicator Deceleration Rate to Avoid the Crash (DRAC), which is well known in the literature (Saccomanno et al., 2008; Fu and Sayed, 2021). This indicator presents the deceleration rate needed to be applied by a vehicle to avoid a collision with another vehicle which can be defined for each vehicle i at the time t as follows:

$$DRAC_i(t) = \frac{(v_i(t) - v_{i-1}(t))^2}{2(p_{i-1}(t) - p_i(t) - L)} \quad (27)$$

Moreover, we consider here the occurrence of hard braking (emergency) maneuver as an additional evaluation scenario where the Leader decelerates from $20m/s$ to $0m/s$ within $20s$. Specifically, results in Fig. 7 show how the platoon reacts in the case of a braking maneuver performed by the leader for each feedback control gain under investigation. Once again, in this case, all CAVs under each control gain smoothly track the motion of the leader during hard braking avoiding possible collisions. It is noteworthy that, although all investigated control parameters can achieve satisfactory tracking performance, only Parameter III stands out as the sole case exhibiting no velocity oscillations, as demonstrated in the results of Section 4.2.1. Furthermore, the selected safety indicator DRACs of different CAVs under different control gains is shown as boxplots in Fig. 8 to explore the changes in the security situation under the hard braking maneuver. It is worth mentioning that the variation of the leader is omitted since it has no predecessor, which raising the risk of collisions. Besides, the CAV2, CAV3, CAV4, and CAV5 refer to the second, third, fourth, and fifth CAV in the CAV platoon, respectively.

From the results presented in Fig. 9, a notable observation is that the DRACs of all CAVs under Parameters II and III are significantly smaller than those under Parameter I, while the DRACs of all CAVs under Parameter IV are greater. This finding suggests that increasing the gain of spacing and velocity errors can lead to a substantial improvement in safety, while increasing the gain of acceleration error exacerbates the DRAC, consistent with the MO results obtained in the tracking performance analysis. Moreover, it is worth noting that, under the same control gain, DRACs decrease significantly with increasing vehicle index. This phenomenon can be attributed to the fact that

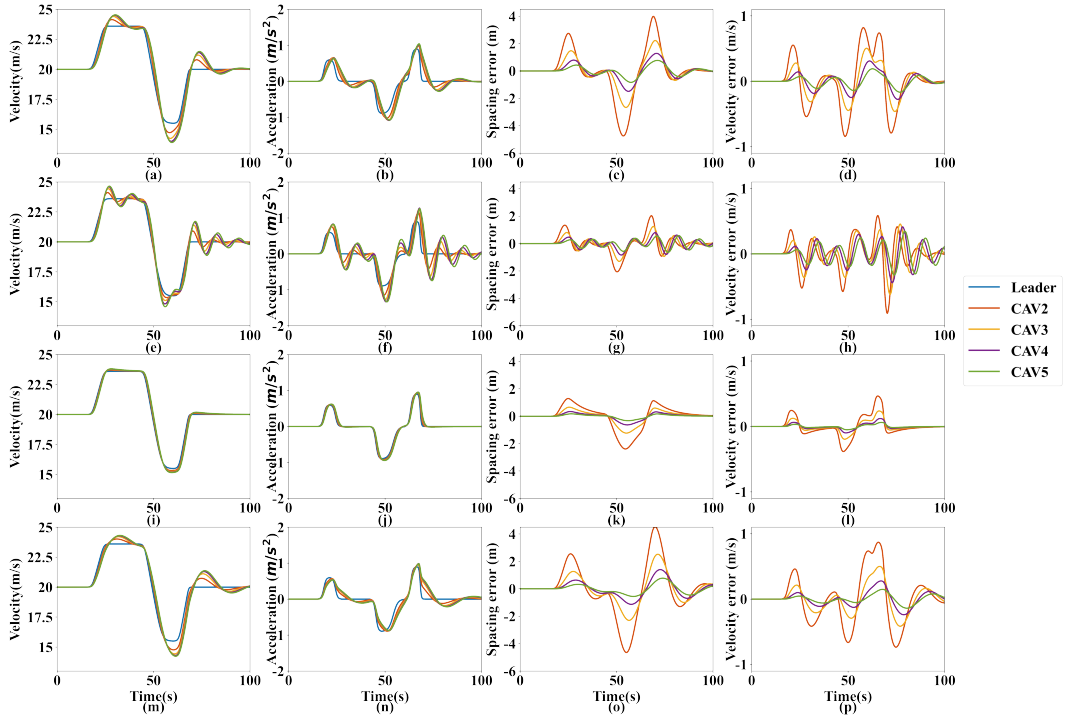


Figure 6: Tracking performance of the CAV platoon for the Trapezoidal signal in Fig. 3(c,d) under the four feedback control gains: (a), (b), (c), and (d) present tracking results under Parameter I, including the velocity, acceleration, tracking error of spacing, and tracking error of velocity, respectively; (e), (f), (g), and (h) show the case under Parameter II; (i), (j), (k), and (l) denote the case under Parameter III; (m), (n), (o), and (p) show the case under Parameter IV.

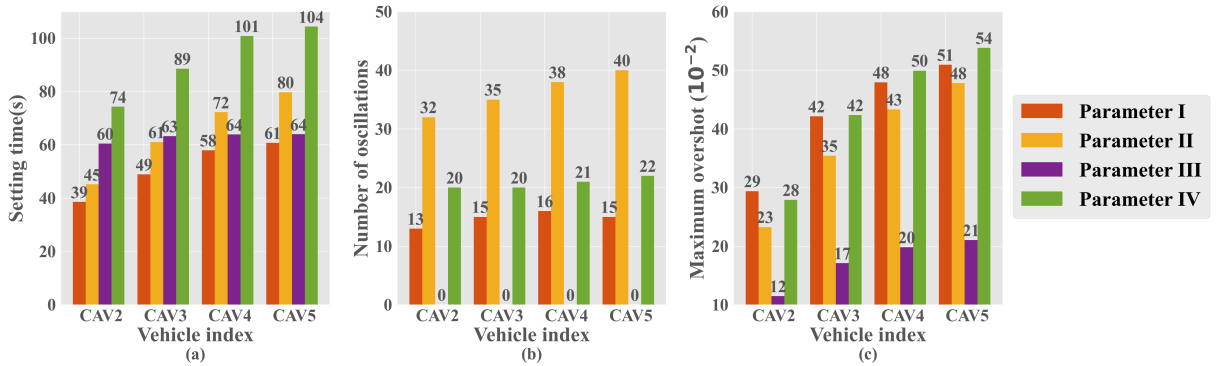


Figure 7: Indicators for evaluating the transient response of each CAV among the CAV platoon under the four feedback control gains: (a) the case of the Setting Time; (b) the case of the Number of Oscillations; (c) the case of the Maximum Overshoot.

Leader-based communication provides CAVs positioned towards the rear of the platoon with access to information further ahead, allowing them to respond to potential dangers at an earlier stage.

4.3. Numerical analyses of the alternative Leader-based IFTs

In this subsection, we investigate the tracking performance of the CAV platoon with alternative IFTs while maintaining the same parameters as those in Table 1 for both network and traffic simulation. Specifically, we set the control gains for the alternative IFTs to the same values: $k_i = [0.3, 0.3, 0.3]^T$. It is worth emphasizing that the control

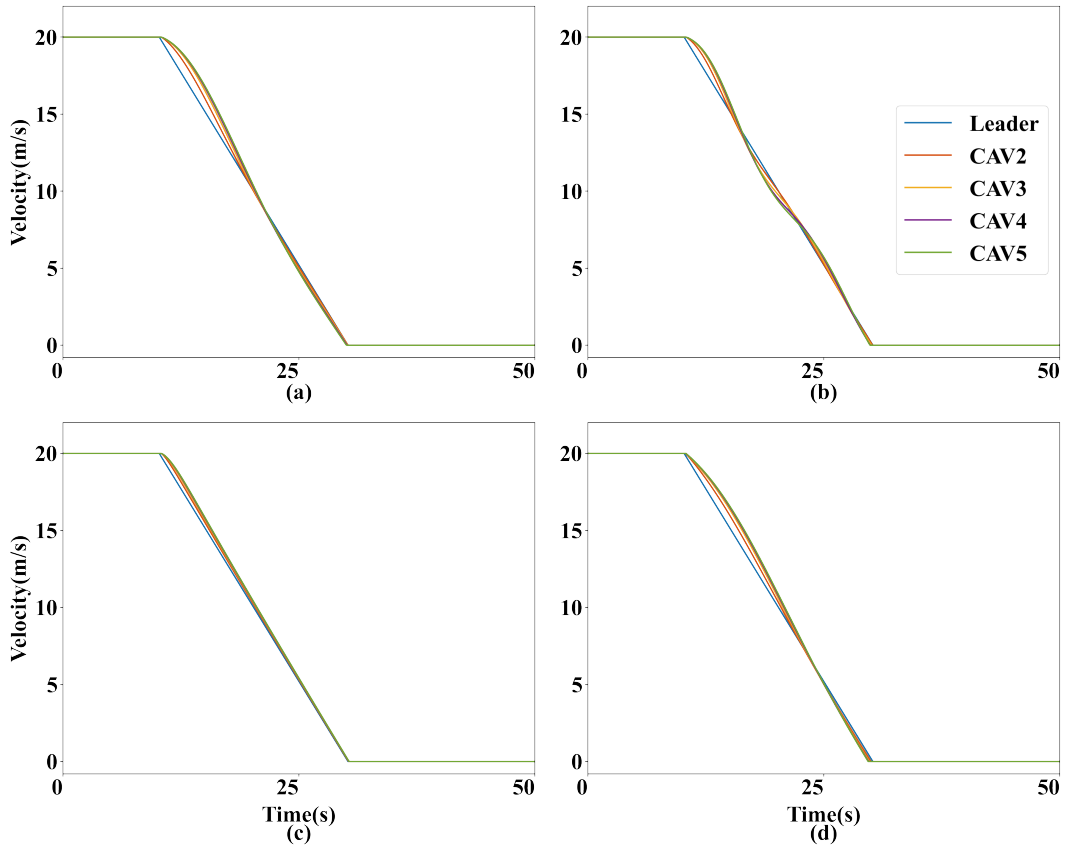


Figure 8: Tracking performance for a hard braking maneuver for each control gain under investigation: (a) Parameter I; (b) Parameter II; (c) Parameter III; (d) Parameter IV.

gains chosen in this section still satisfy the conditions of Theorem 10, which require the existence of matrices P , S , and R , and can be found in Appendix F.

4.3.1. Introduction to the alternative Leader-based IFTs

In this section, we introduce three other widely adopted Leader-based IFTs, namely the Leader-Follower (LF), Leader-Multiple-predecessors-Follower (LMPF), and Leader-Bi-Direction (LBD), as alternative IFTs. Fig. 10 shows the communication schematic of these three Leader-based IFTs, where dotted lines with an arrow indicate one-direction communication, while dotted lines without arrows represent bi-directional communication. For LF, all CAVs in the platoon only obtain information from the leader. In addition, for LMPF, all CAVs in the platoon are able to obtain information from the leader and all predecessors. For LBD, all CAVs in the platoon except the leader are able to obtain information from each vehicle.

4.3.2. Tracking performance analyses for alternative IFTs

As in Section 4.2.1, the Trapezoidal signal defined in Section 4.1 is employed to investigate the tracking performance of different IFTs. The tracking performance of the CAV platoon is presented in Fig. 11.

Alternative IFTs have also been evaluated, and they have demonstrated favorable tracking performance. A similar phenomenon can be observed that the transient response from tracking Leader motion decreases gradually, thanks to stability. It is noteworthy that for the case of LMPF and LBD, the tracking process is smoother, with smaller overshoot and faster setting time. In contrast, for the case of LF, significant velocity oscillations are observed, which negatively impact the tracking performance, as disclosed in the recent technical literature (Zheng et al., 2015).

Correspondingly, the indicators ST, NOO, and MO of different IFTs are also investigated for the transient response analysis, as shown in Fig. 12. The results showed that the LMPF case exhibits almost the best tracking performance in

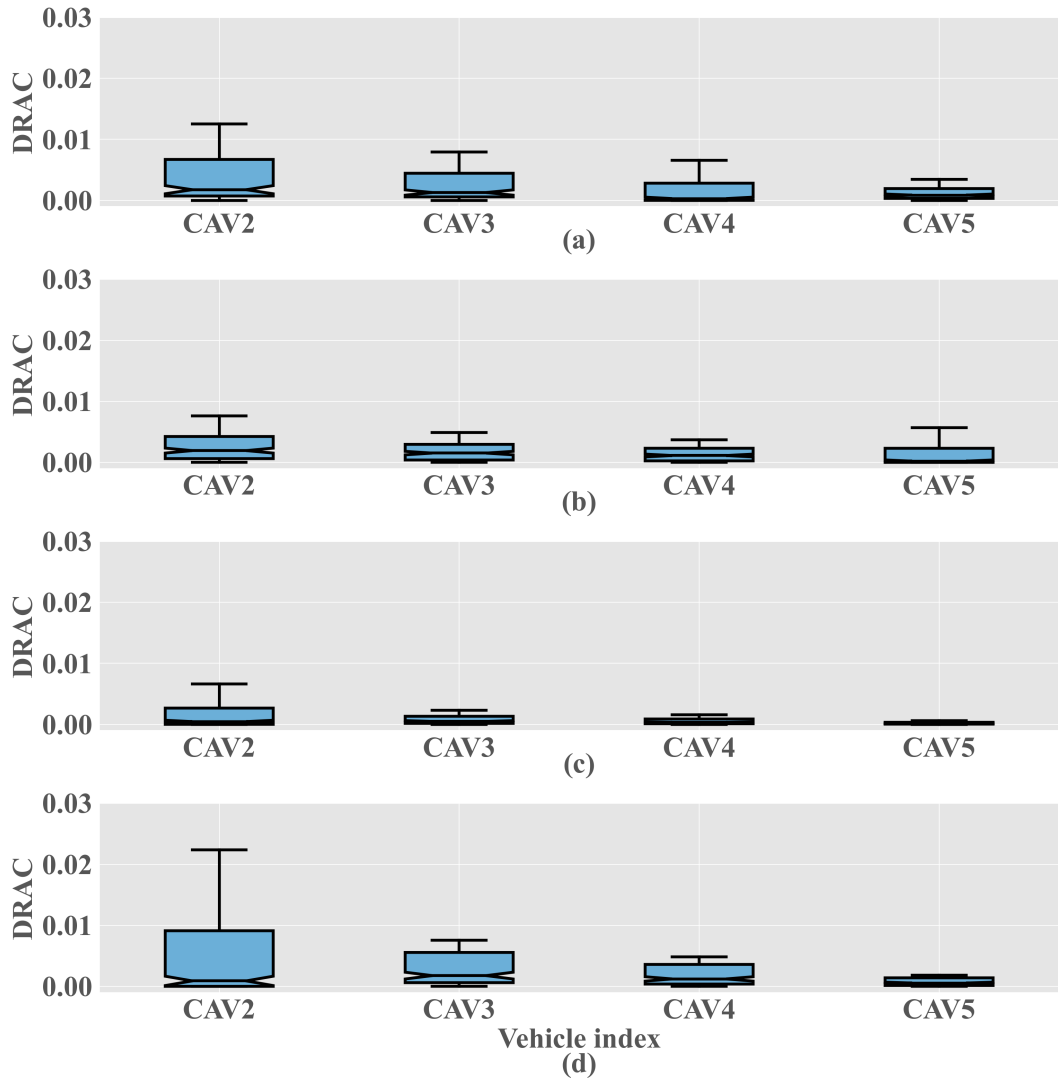


Figure 9: The DRAC boxplots for each CAV of each feedback control gain under investigation: (a) Parameter I; (b) Parameter II; (c) Parameter III; (d) Parameter IV.

all three indicators, indicating that with more communication information, tracking performance can be significantly improved. Conversely, the LF case has the largest MO, NOO, and ST, indicating the worst tracking performance among the four IFTs. The results for the LBD case are more complex. Although it exhibits larger MO and NOO than the LPF case, it can recover from disturbances more quickly. Additionally, it can be inferred that the larger the platoon size, the worse the tracking performance of the CAVs. In summary, having more information can be beneficial for improving tracking performance, but the impact of bi-directional communication is complex.

5. Conclusion and future work

This paper proposes a general supermatrix representation of the CAV platoon under the Leader-based IFT, which considers communication delay and engine actuator delay. To develop this general representation, graph theory is applied to depict communication within the CAV platoon under the Leader-based IFT, and a generic state model is established based on the dynamics of the closed-loop vehicular network using the supermatrices. Additionally, a novel stability condition of the CAV platoon is developed by applying the Bessel-Legendre inequalities and Lyapunov-Krasovskii Stability Theorem based on the general representation. Furthermore, a comprehensive performance

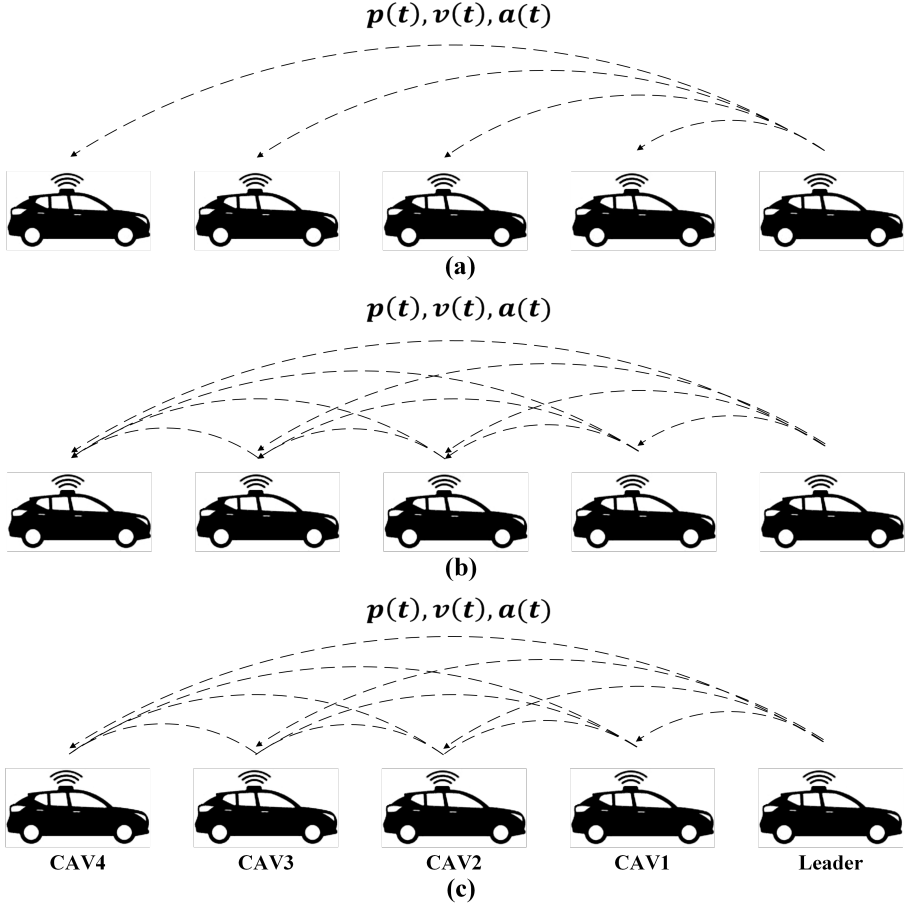


Figure 10: The communication schematic of typical three Leader-based IFTs for the CAV platoon: (a) Leader-Follower (LF); (b) Leader-Multiple-predecessors-Follower (LMPF); and (c) Leader-Bi-Direction (LBD), where dotted lines with an arrow denote the one-direction communication while dotted lines without arrows represent the bi-directional communication.

evaluation analysis of four control parameters is conducted to reveal tracking performance, transient response, and safety conditions in various scenarios, providing guidance for the selection of control parameters. Finally, a comparison of the tracking performance between the CAV platoon employing different IFTs is presented, shedding light on the selection of IFTs. These findings contribute to the development of more effective control strategies for CAV platoons.

The following conclusions can be drawn through numerical analysis:

1. A stability condition that considers multiple time delays for the CAV platoon can be obtained using the Lyapunov-Krasovskii stability theorem and Bessel-Legendre inequalities.
2. The CAV platoon can track the leader motion smoothly, maintain safe conditions in various scenarios, and guarantee stability when employing the investigated control parameters and IFTs.
3. Increasing the gain of velocity errors benefits both tracking performance and safety conditions, while increasing the gain of acceleration errors does not.
4. Increased communication information significantly enhances the tracking and transient performance, whereas the impact of adopting bi-directional communication is complex.

Admittedly, we acknowledge that the vehicle behavior simulated in this study is a simplified version of real-world scenarios, and further field tests with more realistic vehicle dynamics models are needed to validate our findings. Additionally, this paper focuses only on the CD policy while the Constant Time Headway policy is also widely used and requires further investigation. Furthermore, while this study mainly examines Leader-based IFTs, there is a need to extend the analysis to more general IFTs. Another area of future research is to investigate communication delays

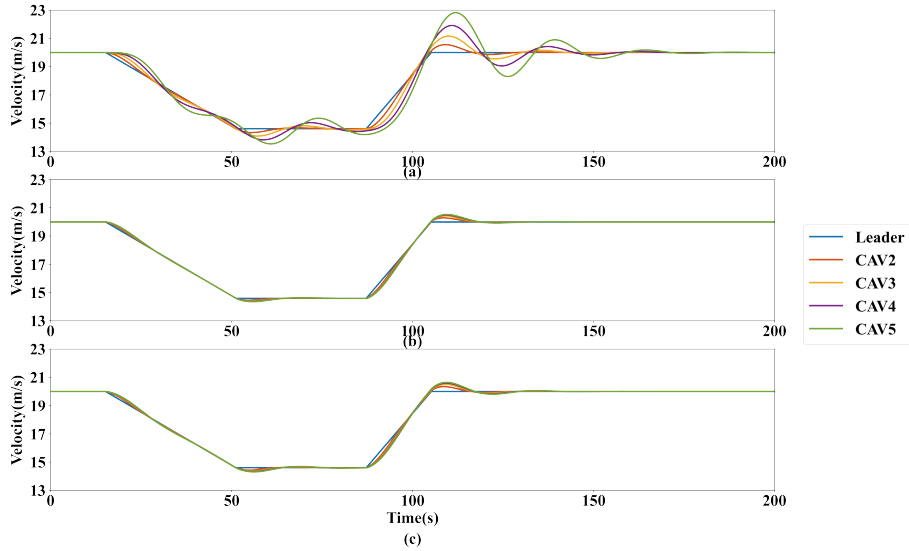


Figure 11: Tracking performance of the CAV platoon for the Trapezoidal signal in Fig. 3(a,b) under the alternative three IFTs: (a) presents tracking results under LF; (b) presents tracking results under LMPF; (c) denotes the case under LBD.

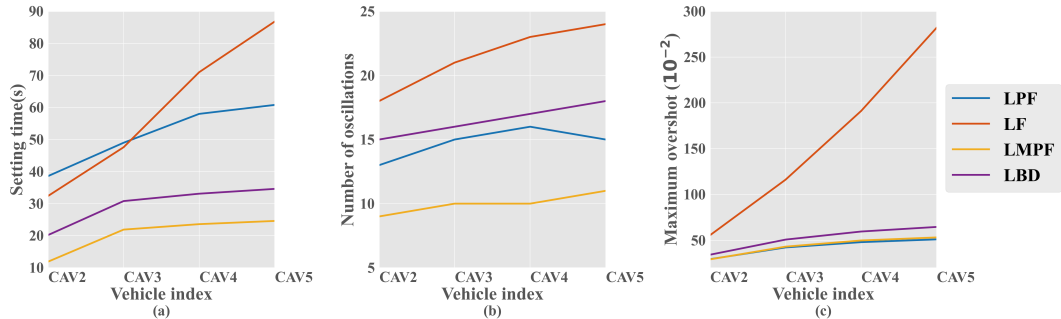


Figure 12: Indicators for evaluating the transient response of each CAV among the CAV platoon under the four IFTs: (a) the case of Setting Time; (b) the case of the Number of Oscillations; (c) the case of Maximum Overshoot.

further since the assumed upper bound is constant for simplification, whereas communication delays are typically time-varying and depend on the surrounding environment. Therefore, future work should be directed toward developing a novel stability theorem to address time-varying communication delays. Moreover, the control parameter scheme that yields optimal tracking performance should be further investigated through theoretical research and field experiments. Finally, future research should also focus on designing novel control strategies to enable smoother and safer tracking performance.

Appendix A. Proof of Lemma 6

Assuming a function $x \in C$, a positive definite matrix $R \in \mathbb{S}_n^+$, and $h > 0$, the approximation error between $x(u)$ and its projection onto the orthogonal sequence set $\{\mathcal{L}_k, k \in \mathbb{N}\}$ with respect to the inner product can be expressed as:

$$y_N(u) = x(u) - \sum_{k=0}^N \frac{\int_{-h}^0 \mathcal{L}_k(u)x(u)du}{\int_{-h}^0 \mathcal{L}_k^2(u)du} \mathcal{L}_k(u) = x(u) - \sum_{k=0}^N \frac{2k+1}{h} \Omega_k \mathcal{L}_k(u) \quad (28)$$

Clearly, it follows that $y_N \in \mathcal{C}$. Furthermore, the integral $\int_{-h}^0 y_N^T(u) R y_N(u) du$ exists, and the orthogonality property (15) implies:

$$\begin{aligned} \int_{-h}^0 y_N^T(u) R y_N(u) du &= \int_{-h}^0 x^T(u) R x(u) du \\ &\quad - 2 \sum_{k=0}^N \frac{2k+1}{h} \left(\int_{-h}^0 \mathcal{L}_k(u) x(u) du \right)^T R \Omega_k(x) \\ &\quad + \sum_{k=0}^N \left(\frac{2k+1}{h} \right)^2 \left(\int_{-h}^0 \mathcal{L}_k^2(u) du \right) \Omega_k^T(x) R \Omega_k(x). \end{aligned} \quad (29)$$

According to the definition, some derivation can be provided:

$$\begin{cases} \Omega_k(x) = \int_{-h}^0 \mathcal{L}_k(u) x(u) du \\ \left(\frac{2k+1}{h} \right)^2 \int_{-h}^0 \mathcal{L}_k^2(u) du = \frac{2k+1}{h} \end{cases} \quad (30)$$

Substituting the above Equation into Equation (29), we get:

$$\int_{-h}^0 y_N^T(u) R y_N(u) du = \int_{-h}^0 x^T(u) R x(u) du - \sum_{k=0}^N \frac{2k+1}{h} \Omega_k^T(x) R \Omega_k(x). \quad (31)$$

The inequality (19) can be established by recognizing that $\int_{-h}^0 z_N^T(u) R z_N(u) du > 0$ for any positive definite matrix R .

Appendix B. Feedback control for linearization

In this appendix, we provide the linearization of the longitudinal vehicle dynamic in Equation (1). The functions of the lumped uncertain resistance forces, including $f_i^g(t)$, $f_i^w(t)$, and $f_i^r(t)$ are expressed as follows:

$$\begin{cases} f_i^g(t) = m_i g \sin(\theta_i(t)) \\ f_i^w(t) = \frac{1}{2} \rho C_D A_F (v_i(t) + v_w(t))^2 \\ f_i^r(t) = \mu_R m_i g \cos(\theta_i(t)) \end{cases} \quad (32)$$

where $g = 9.81 m/s^2$ denotes the acceleration of gravity; $\theta_i(t)$ is the inclination angle of the road; ρ denotes the air density; C_D is the aerodynamic drag coefficient; A_F represents the maximal cross-sectional/frontal area of the vehicle; $v_w(t)$ denotes the uncertain headwind speed; μ_R is the coefficient of rolling resistance.

The desired engine dynamic is modeled as follows:

$$(\tau_i s + 1) F_i^e = U_i \quad (33)$$

Adopting the inverse Laplace transformation on Equation (33) arrives at:

$$\dot{f}_i^e(t) = \frac{u_i(t)}{\tau_i} - \frac{f_i^e(t)}{\tau_i} \quad (34)$$

Substituting Equation (1) into Equation (34) and differentiating both sides of Equation (34) with respect to time, we get:

$$\begin{aligned}\dot{a}_i(t) &= \frac{\dot{f}_l^e(t)}{m_i} - \frac{\dot{f}_l^g(t)}{m_i} - \frac{\dot{f}_l^{i\omega}(t)}{m_i} - \frac{\dot{f}_l^r(t)}{m_i} \\ &= \frac{u_i(t)}{m_i \tau_i} \\ &\quad - \frac{a_i(t) + g \sin(\theta_i(t)) [1 - \tau_i \mu_R \dot{\theta}_i(t)] + g \cos(\theta_i(t)) [1 + \tau_i \dot{\theta}_i(t)]}{\tau_i} \\ &\quad - \frac{\frac{1}{2} \rho C_D A_F (v_i(t) + v_w(t)) ((v_i(t) + v_w(t)) + 2\tau_i (a_i(t) + \dot{v}_w(t)))}{\tau_i}\end{aligned}\tag{35}$$

Thus, the nonlinear state feedback chosen for linearizing can be defined by:

$$\begin{aligned}u_i^*(t) &= m_i u_i(t) + g \sin(\theta_i(t)) [1 - \tau_i \mu_R \dot{\theta}_i(t)] + g \cos(\theta_i(t)) [1 + \tau_i \dot{\theta}_i(t)] \\ &\quad + \frac{1}{2} \rho C_D A_F (v_i(t) + v_w(t)) ((v_i(t) + v_w(t)) + 2\tau_i (a_i(t) + \dot{v}_w(t)))\end{aligned}\tag{36}$$

Under the new feedback control input, the Equation (1) can be rewritten as:

$$\tau_i \dot{a}_i(t) + a_i(t) = u_i(t)\tag{37}$$

Appendix C. Proof of Corollary 9

Applying Lemma 6 to the order N , we get:

$$\int_{-h}^0 \dot{x}^T(u) R \dot{x}(u) du \geq \frac{1}{h} \begin{bmatrix} \Omega_0(\dot{x}) \\ \Omega_1(\dot{x}) \\ \vdots \\ \Omega_N(\dot{x}) \end{bmatrix}^T R_N \begin{bmatrix} \Omega_0(\dot{x}) \\ \Omega_1(\dot{x}) \\ \vdots \\ \Omega_N(\dot{x}) \end{bmatrix}\tag{38}$$

An integration by parts of $\Omega_k(\dot{x})$ ensures that, for all $k \geq 0$:

$$\Omega_k(\dot{x}) = \mathcal{L}_k(0)x(0) - \mathcal{L}_k(-h)x(-h) - \int_{-h}^0 \left(\frac{d}{du} \mathcal{L}_k(u) \right) x(u) du\tag{39}$$

Substituting the Boundary conditions (16) and Differentiation (17) into $\Omega_k(\dot{x})$, we get:

$$\Omega_k(\dot{x}) = x(0) - (-1)^k x(-h) + \sum_{i=0}^{k-1} \frac{\gamma_{Nk}^i}{h} \Omega_i(x) = \Gamma_N(k) \xi_N\tag{40}$$

Replacing $\Omega_k(\dot{x})$ by $\Gamma_N(k) \xi_N$ leads to Equation (23).

Appendix D. Proof of Theorem 10

According to the Corollary 9, the states of system need to be extended to $\tilde{x}_N(t)$ defined as:

$$\tilde{x}_N(t) = \begin{bmatrix} x_t(0) \\ \int_{-h}^0 \mathcal{L}_0(s) x_t(s) ds \\ \vdots \\ \int_{-h}^0 \mathcal{L}_{N-1}(s) x_t(s) ds \\ x_t(0), \end{bmatrix} = \begin{bmatrix} x_t(0) \\ \Omega_0(x_t) \\ \vdots \\ \Omega_{N-1}(x_t) \\ x_t(0), \end{bmatrix}, \quad \text{if } N \geq 1, \quad \text{if } N = 0.\tag{41}$$

The augmented vector $\tilde{x}_N(t)$ is constructed by stacking the instantaneous state $x_t(0)$ with the projections of the state function x_t onto the first N Legendre polynomials. By performing an integration by parts, the time derivative of $\tilde{x}_N(t)$ can be expressed as follows, as shown in Appendix C:

$$\dot{\tilde{x}}_N(t) = H_N \xi_N(t) \quad (42)$$

where

$$\xi_N(t) = \begin{cases} \begin{bmatrix} x_t^T(0) \\ x_t^T(-h) \\ \frac{1}{h} \int_{-h}^0 \mathcal{L}_0(s)x_t(s)ds \\ \vdots \\ \frac{1}{h} \int_{-h}^0 \mathcal{L}_{N-1}(s)x_t(s)ds \end{bmatrix}, & \text{if } N \geq 1 \\ \begin{bmatrix} x_t^T(0) \\ x_t^T(-h) \end{bmatrix}, & \text{if } N = 0 \end{cases} \quad (43)$$

It should be noted that the states of the argument system consist of both the states of the original delay system and those of the Linear Time-Invariant (LTI) system. Additionally, Equation (42) only contains one delay term, namely $x_t(-h)$, which allows for the selection of the LKF as follows:

$$V_N(x_t, \dot{x}_t) = \tilde{x}_N^T(t)P_N\tilde{x}_N(t) + \int_{t-h}^t x^T(s)Sx(s)ds + h \int_{t-h}^t \int_\theta^t \dot{x}^T(s)R\dot{x}(s)dsd\theta \quad (44)$$

Applying Lemma 6 to Equation (44) yields:

$$V_N(x_t, \dot{x}_t) \geq \tilde{x}_N^T(t)\Theta_N(h)\tilde{x}_N(t) + h \int_{t-h}^t \int_\theta^t \dot{x}^T(s)R\dot{x}(s)dsd\theta \quad (45)$$

The positive definiteness of V_N is ensured by ensuring that $S > 0$, $R > 0$, and $\Theta_N(h) > 0$. In addition, for a sufficiently small $\varepsilon_1 > 0$, $\Theta_N(h) \succ [\varepsilon_1 I \ 0 \ 0 \ 0]$, which implies that $V_N(x_t, \dot{x}_t) \geq \varepsilon_1 |x_t(0)|^2$. Moreover, it is guaranteed that $P_N \prec \lambda \text{diag}(I, I, 3I, 5I, \dots, (2N-1)I)$ for a sufficiently large scalar $\lambda > 0$. As a result, we have:

$$\begin{aligned} V_N(x_t, \dot{x}_t) &\leq \lambda |x_t(0)|^2 + \lambda \sum_{i=0}^{N-1} (2i+1)\Omega_i^T \Omega_i + \int_{t-h}^t x^T(s)Sx(s)ds \\ &\quad + h \int_{t-h}^t \int_\theta^t \dot{x}^T(s)R\dot{x}(s)dsd\theta \end{aligned} \quad (46)$$

According to Lemma 6, we get:

$$\begin{aligned} V_N(x_t, \dot{x}_t) &\leq \lambda |x_t(0)|^2 + \int_{t-h}^t x^T(s)(\lambda h I + S)x(s)ds \\ &\quad + h \int_{t-h}^t \int_\theta^t \dot{x}^T(s)R\dot{x}(s)dsd\theta \end{aligned} \quad (47)$$

which guarantees that there exists a scalar $\varepsilon_2 > 0$, such that $V_N(x_t, \dot{x}_t) \leq \varepsilon_2 |\bar{x}_t|_h^2$ holds for $\forall t > h$, where $\bar{x}_t = \begin{bmatrix} x_t \\ \dot{x}_t \end{bmatrix}$.

Then it holds:

$$\varepsilon_1 |x_t(0)|^2 \leq V_N(x_t, \dot{x}_t) \leq \varepsilon_2 |\bar{x}_t|_h^2. \quad (48)$$

After that, consider the derivative of V_N for all $t \geq h$, we obtain:

$$\begin{aligned} \dot{V}_N(x_t, \dot{x}_t) &= 2\tilde{x}_N^T(t)P_N\dot{\tilde{x}}_N(t) + x_t^T(0)Sx_t(0) \\ &\quad - x_t^T(-h)Sx_t(-h) + h^2 \dot{x}_t^T(0)R\dot{x}_t(0) \\ &\quad - h \int_{-h}^0 \dot{x}_t^T(s)R\dot{x}_t(s)ds. \end{aligned} \quad (49)$$

Substituting $\tilde{x}_N(t) = G_N(h)\xi_N(t)$, $\dot{\tilde{x}}_N(t) = H_N\xi_N(t)$, and $\dot{x}_t(0) = F_N\xi_N(t)$, we get:

$$\dot{V}_N(x_t, \dot{x}_t) = \xi_N^T(t)\Phi_{N0}(h)\xi_N(t) - h \int_{-h}^0 \dot{x}_t^T(s)R\dot{x}_t(s)ds \quad (50)$$

Applying the Corollary 9 to the order N and injecting the resulting inequality (23) into Equation (50) leads to:

$$\dot{V}_N(x_t, \dot{x}_t) \leq \xi_N^T(t)\Phi_N(h)\xi_N(t) \quad (51)$$

Hence, if the LMIs (25) are satisfied, there exists a scalar $\varepsilon_3 > 0$ such that $\Phi_N(h) \prec \begin{bmatrix} -\varepsilon_3 I & 0 \\ 0 & 0 \end{bmatrix}$. Therefore, the following inequality holds:

$$\dot{V}_N(x_t, \dot{x}_t) \leq -\varepsilon_3 |x_t(0)|^2, \quad \forall t \geq h \quad (52)$$

The inequality (52) ensures the negative definiteness of \dot{V}_N . As for the stability of system (12), by integrating inequality (52), we get:

$$V_N(x_t, \dot{x}_t) - V_N(x_h, \dot{x}_h) \leq -\varepsilon_3 \int_h^t |x_s(0)|^2 ds \quad (53)$$

and, hence, Equation (53) yields:

$$\varepsilon_1 |x_t(0)|^2 \leq V_N(x_t, \dot{x}_t) \leq V_N(x_h, \dot{x}_h) \leq \varepsilon_2 |\bar{x}_h|^2 \quad (54)$$

Since $|x_h|_h \leq c_1 |\phi|_h$, $c_1 > 0$ (Hale and Lunel, 2013) and $|\dot{x}_h|_h \leq c_2 |\phi|_h$, $c_2 > 0$ according to the definition in Equation (12), we obtain that:

$$|x_t(0)|^2 \leq \frac{V_N(x_h, \dot{x}_h)}{\varepsilon_1} \leq c_3 |\phi|_h^2, \quad c_3 > 0 \quad (55)$$

Therefore, system (12) can be proven to be stable. To establish asymptotic stability, it is noted that, for any initial condition ϕ , x is uniformly continuous on $[0, \infty)$ since x defined by the right-hand side of system (12) is uniformly bounded. Additionally, the integrability of $|x_t(0)|^2$ on $[h, \infty)$ can be concluded from Equation (53). Hence, according to Barbalat's lemma (Min and Liu, 2007), $x_t(0)$ approaches zero as t approaches infinity. Therefore, if the LMI of Theorem 10 are satisfied, the delay system (12) is asymptotically stable for the constant delay h .

Appendix E. Connection between Lyapunov-Krasovskii stability theorem and Second Lyapunov method.

First, we present a lemma on the Lyapunov function:

Lemma 14 ((Kolmanovskii and Myshkis, 1999)) Let a system $\dot{X}(t) = f(x(t), X(t-h))$ with $f(0, 0) = 0$. Assume the Lyapunov function $F : G \rightarrow \mathbb{R}$ exists with $X, y \in G$, $F(y) < F(X)$ implies

$$(\dot{F}(X)f(X, y))(\ddot{F}(X)f(X, y)) \leq 0. \quad (56)$$

Then the solution $X(t) \equiv 0$ is stable.

Suppose there exists a Lyapunov function $F : \mathbb{R}^n \rightarrow \mathbb{R}$. Then define functional $V : \mathcal{C} \rightarrow \mathbb{R}$ as follows:

$$V(\phi) := \max_{-h \leq \theta \leq 0} F(\phi(\theta)), (\forall \phi \in \mathcal{C}). \quad (57)$$

By definition, the following conditions hold:

$$\dot{V}(\phi) \left\{ \begin{array}{ll} \leq 0, & \text{if } F(\phi(0)) < V(\phi), \\ = \max(\dot{F}(\phi(0)), f(\phi(0), \phi(-h)), 0), & \text{if } F(\phi(0)) = V(\phi), \end{array} \right. \quad (58)$$

where $f(\phi(0), \phi(-h)) = A^* \phi(0) + \Psi \phi(-h)$.

Thus $\dot{V}(\phi) > 0$ holds if and only if the following condition holds:

$$F(\phi(0)) = \max_{-h \leq \theta \leq 0} F(\phi(\theta)) \text{ and } (\dot{F}(\phi(0)), f(\phi(0), \phi(-h))) > 0. \quad (59)$$

The function F can be defined in some neighborhood $G \subset \mathbb{R}^n$. And the functional V is then defined for $\phi \in C$ with values in G .

Suppose Equation (59) holds for some functions $\phi \in C$, then we can obtain the inequality $F(\phi(-h)) < F(\phi(0))$ making ϕ arbitrarily small. Thus the second condition in Equation (59) still holds, but conflicts with Lemma 14. Therefore $\dot{V}(\phi) \leq 0$ holds constantly for all ϕ .

It can be concluded that the Lyapunov-Krasovskii stability theorem can be considered as an extension of the Second Lyapunov method to functional space. This extension does not introduce any additional constraints since it only constrains the definite sign at the start and end points instead of in the neighborhood. As a result, the stability conditions obtained using the Lyapunov-Krasovskii stability theorem are more accurate than those obtained using the Second Lyapunov method. This conclusion has been supported by previous research (Wang et al., 2016; Lian et al., 2020).

Appendix F. Attachments uploaded to GitHub

The uploaded code for this paper includes the formulation of Theorem 1 and the construction of LMIs for Theorem 10. Additionally, matrices corresponding to the four sets of control parameters for LPF, as selected in Section 4.2, and three sets for LF, LMPF, and LBD, as selected in Section 4.3, which are compatible with Theorem 10, have been included in the repository. The file repository URL is: <https://github.com/ruantiancheng/code-paper-7>.

CRediT authorship contribution statement

Tiancheng Ruan: Conceptualization of this study, Methodology, Writing - Original draft preparation, Resources, Software. **Hao Wang:** Formal analysis, Funding acquisition, Supervision, Writing - review & editing. **Xiaopeng Li:** Writing - Original draft preparation, Writing - review & editing. **Yujia Chen:** Writing - Original draft preparation. **Changyin Dong:** Formal analysis, Funding acquisition.

Acknowledgment

This research was sponsored by the National Key Research and Development Program of China (No. 2022ZD0115600), National Science Foundation of China (No. 52072067), Postgraduate Research & Practice Innovation Program of Jiangsu Province (KYCX22_0266).

References

- Abbas, F., Fan, P., Khan, Z., 2018. A novel low-latency V2V resource allocation scheme based on cellular V2X communications. *IEEE Transactions on Intelligent Transportation Systems* 20, 2185–2197.
- Abdallah, C.T., Sipahi, R., Niculescu, S.J., Michiels, W., Gu, K., 2011. Stability and stabilization of systems with time delay: limitations and opportunities. *IEEE Transactions on Control Systems Technology* 31, 38.
- van Arem, B., Abbas, M.M., Li, X., Head, L., Zhou, X., Chen, D., Bertini, R., Mattingly, S.P., Wang, H., Orosz, G., 2016. Integrated traffic flow models and analysis for automated vehicles, in: *Road Vehicle Automation 3*. Springer, pp. 249–258.
- Bos, L., Narayan, A., Levenberg, N., Piazzon, F., 2017. An orthogonality property of the legendre polynomials. *Constructive Approximation* 45, 65–81.
- Chandler, R.E., Herman, R., Montroll, E.W., 1958. Traffic dynamics: studies in car following. *Operations research* 6, 165–184.
- Chang, X., Li, H., Rong, J., Zhao, X., 2020. Analysis on traffic stability and capacity for mixed traffic flow with platoons of intelligent connected vehicles. *Physica A: Statistical Mechanics and its Applications* 557, 124829.
- Chen, T., Wang, M., Gong, S., Zhou, Y., Ran, B., 2021. Connected and automated vehicle distributed control for on-ramp merging scenario: A virtual rotation approach. *Transportation Research Part C: Emerging Technologies* 133, 103451.
- Dattoli, G., Ricci, P.E., Cesarano, C., 2001. A note on legendre polynomials. *International Journal of Nonlinear Sciences and Numerical Simulation* 2, 365–370.
- Dey, K.C., Yan, L., Wang, X., Wang, Y., Shen, H., Chowdhury, M., Yu, L., Qiu, C., Soundararaj, V., 2015. A review of communication, driver characteristics, and controls aspects of cooperative adaptive cruise control (CACC). *IEEE Transactions on Intelligent Transportation Systems* 17, 491–509.
- Dragomir, S.S., 2001. A note on bessel's inequality. *RGMIA research report collection* 4.

- Eyre, J., Yanakiev, D., Kanellakopoulos, I., 1998. A simplified framework for string stability analysis of automated vehicles. *Vehicle System Dynamics* 30, 375–405.
- Fridman, E., 2006. Descriptor discretized lyapunov functional method: analysis and design. *IEEE Transactions on Automatic control* 51, 890–897.
- Fridman, E., 2014. Tutorial on lyapunov-based methods for time-delay systems. *European Journal of Control* 20, 271–283.
- Fridman, E., Pila, A., Shaked, U., 2003. Regional stabilization and H_∞ control of time-delay systems with saturating actuators. *International Journal of Robust and Nonlinear Control: IFAC-Affiliated Journal* 13, 885–907.
- Fu, C., Sayed, T., 2021. Comparison of threshold determination methods for the deceleration rate to avoid a crash (drac)-based crash estimation. *Accident Analysis & Prevention* 153, 106051.
- Gao, F., Li, S.E., Zheng, Y., Kum, D., 2016. Robust control of heterogeneous vehicular platoon with uncertain dynamics and communication delay. *IET Intelligent Transport Systems* 10, 503–513.
- Gazis, D.C., Herman, R., Rothery, R.W., 1963. Analytical methods in transportation: Mathematical car-following theory of traffic flow. *Journal of the Engineering Mechanics Division* 89, 29–46.
- Ghiasi, A., Hussain, O., Qian, Z.S., Li, X., 2017. A mixed traffic capacity analysis and lane management model for connected automated vehicles: A Markov chain method. *Transportation Research Part B: Methodological* 106, 266–292.
- Gouaisbaut, F., Peaucelle, D., 2006. A note on stability of time delay systems. *IFAC Proceedings Volumes* 39, 555–560.
- Gu, K., Chen, J., Kharitonov, V.L., 2003. Stability of time-delay systems. Springer Science & Business Media.
- Gu, K., Liu, Y., 2009. Lyapunov–Krasovskii functional for uniform stability of coupled differential-functional equations. *Automatica* 45, 798–804.
- Hale, J.K., Lunel, S.M.V., 2013. Introduction to functional differential equations. volume 99. Springer Science & Business Media.
- Hengster-Movric, K., Lewis, F.L., Šebek, M., Vyhlídal, T., 2015. Cooperative synchronization control for agents with control delays: A synchronizing region approach. *Journal of the Franklin Institute* 352, 2002–2028.
- Herman, R., Montroll, E.W., Potts, R.B., Rothery, R.W., 1959. Traffic dynamics: analysis of stability in car following. *Operations research* 7, 86–106.
- Hua, X., Yu, W., Wang, W., 2022. Stability analysis of heterogeneous traffic flow with connected and automated vehicles: Joint consideration of communication failures and driver takeover. *Journal of Advanced Transportation* 2022.
- Jarrett, D., Xiaoyan, Z., 1993. The dynamic behaviour of road traffic flow: stability or chaos?, in: *Applications of Fractals and Chaos: The Shape of Things*, Springer. pp. 237–248.
- Jin, I.G., Orosz, G., 2016. Optimal control of connected vehicle systems with communication delay and driver reaction time. *IEEE Transactions on Intelligent Transportation Systems* 18, 2056–2070.
- Kamath, G.K., Jagannathan, K., Raina, G., 2015. Car-following models with delayed feedback: local stability and hopf bifurcation, in: 2015 53rd Annual Allerton Conference on Communication, Control, and Computing (Allerton), IEEE. pp. 538–545.
- Kolmanovskii, V., Myshkis, A., 1999. *Introduction to the Theory and Applications of Functional Differential Equations*. Springer Netherlands, Dordrecht. doi:10.1007/978-94-017-1965-0.
- Lee, W.I., Lee, S.Y., Park, P., 2018. Affine Bessel–Legendre inequality: Application to stability analysis for systems with time-varying delays. *Automatica* 93, 535–539.
- Lhachemi, H., Prieur, C., 2020. Feedback stabilization of a class of diagonal infinite-dimensional systems with delay boundary control. *IEEE Transactions on Automatic Control* 66, 105–120.
- Li, Y., Li, K., Cai, L., Zhu, H., Sun, F., 2016. Feedback-based platoon control for connected autonomous vehicles under different communication network topologies, in: 2016 35th Chinese Control Conference (CCC), pp. 8806–8811. doi:10.1109/ChiCC.2016.7554764.
- Li, Y., Wang, H., Wang, W., Xing, L., Liu, S., Wei, X., 2017. Evaluation of the impacts of cooperative adaptive cruise control on reducing rear-end collision risks on freeways. *Accident Analysis & Prevention* 98, 87–95.
- Li, Y., Wu, G., Zhu, H., Tang, X., 2019. Stability analysis for car-following model considering position error, in: 2019 IEEE 8th Data Driven Control and Learning Systems Conference (DDCLS), pp. 861–865.
- Lian, H.H., Xiao, S.P., Yan, H., Yang, F., Zeng, H.B., 2020. Dissipativity analysis for neural networks with time-varying delays via a delay-product-type lyapunov functional approach. *IEEE transactions on neural networks and learning systems* 32, 975–984.
- Martín-Sacristán, D., Roger, S., García-Roger, D., Monserrat, J.F., Spapis, P., Zhou, C., Kaloxyllos, A., 2020. Low-Latency Infrastructure-Based Cellular V2V Communications for Multi-Operator Environments With Regional Split. *IEEE Transactions on Intelligent Transportation Systems* 22, 1052–1067.
- Milanés, V., Shladover, S.E., Spring, J., Nowakowski, C., Kawazoe, H., Nakamura, M., 2013. Cooperative adaptive cruise control in real traffic situations. *IEEE Transactions on intelligent transportation systems* 15, 296–305.
- Min, Y.Y., Liu, Y.G., 2007. Barbalat lemma and its application in analysis of system stability. *Journal of Shandong University (engineering science)* 37, 51–55.
- Montanino, M., Punzo, V., 2021. On string stability of a mixed and heterogeneous traffic flow: A unifying modelling framework. *Transportation Research Part B: Methodological* 144, 133–154.
- Navas, F., Milanés, V., 2019. Mixing V2V- and non-V2V-equipped vehicles in car following. *Transportation Research Part C: Emerging Technologies* 108, 167–181. URL: <https://doi.org/10.1016/j.trc.2019.08.021>. doi:10.1016/j.trc.2019.08.021.
- Ogata, K., 1995. *Discrete-time control systems*. Prentice-Hall, Inc.
- Park, P., Lee, W.I., Lee, S.Y., 2015. Auxiliary function-based integral inequalities for quadratic functions and their applications to time-delay systems. *Journal of the Franklin Institute* 352, 1378–1396.
- Pirani, M., Baldi, S., Johansson, K.H., 2022. Impact of Network Topology on the Resilience of Vehicle Platoons. *IEEE Transactions on Intelligent Transportation Systems*.
- Qin, Y., Wang, H., Ran, B., 2018. Stability Analysis of Connected and Automated Vehicles to Reduce Fuel Consumption and Emissions. *Journal of Transportation Engineering, Part A: Systems* 144, 04018068. doi:10.1061/jtpebs.0000196.

- Razzaghpoor, M., Shahram, S., Valiente, R., Fallah, Y.P., 2021. Impact of communication loss on mpc based cooperative adaptive cruise control and platooning, in: 2021 IEEE 94th Vehicular Technology Conference (VTC2021-Fall), IEEE. pp. 01–07.
- Ruan, T., Wang, H., Zhou, L., Zhang, Y., Dong, C., Zuo, Z., 2022. Impacts of information flow topology on traffic dynamics of cav-mv heterogeneous flow. *IEEE Transactions on Intelligent Transportation Systems*, 1–16doi:10.1109/TITS.2022.3170965.
- Ruan, T., Zhou, L., Wang, H., 2021. Stability of heterogeneous traffic considering impacts of platoon management with multiple time delays. *Physica A: Statistical Mechanics and its Applications* 583, 126294.
- Saccomanno, F.F., Cunto, F., Guido, G., Vitale, A., 2008. Comparing safety at signalized intersections and roundabouts using simulated rear-end conflicts. *Transportation Research Record* 2078, 90–95.
- Sarker, A., Shen, H., Rahman, M., Chowdhury, M., Dey, K., Li, F., Wang, Y., Narman, H.S., 2019. A review of sensing and communication, human factors, and controller aspects for information-aware connected and automated vehicles. *IEEE transactions on intelligent transportation systems* 21, 7–29.
- Schrank, D., Eisele, B., Lomax, T., 2012. TTI's 2012 urban mobility report. Texas A&M Transportation Institute. The Texas A&M University System 4.
- Seuret, A., Gouaisbaut, F., 2013. Wirtinger-based integral inequality: application to time-delay systems. *Automatica* 49, 2860–2866.
- Sun, J., Zheng, Z., Sun, J., 2018. Stability analysis methods and their applicability to car-following models in conventional and connected environments. *Transportation research part B: methodological* 109, 212–237. Publisher: Elsevier.
- Thota, J., Abdulla, N.F., Doufexi, A., Armour, S., 2019. V2V for vehicular safety applications. *IEEE Transactions on Intelligent Transportation Systems* 21, 2571–2585.
- Verizon North, L.L.C., 2020. Federal Communications Commission. Proceeding Number 19, 354.
- Vu, H.V., Liu, Z., Nguyen, D.H.N., Morawski, R., Le-Ngoc, T., 2020. Multi-agent reinforcement learning for joint channel assignment and power allocation in platoon-based C-V2X systems. arXiv preprint arXiv:2011.04555 .
- Vukadinovic, V., Bakowski, K., Marsch, P., Garcia, I.D., Xu, H., Sybis, M., Sroka, P., Wesolowski, K., Lister, D., Thibault, I., 2018. 3GPP C-V2X and IEEE 802.11p for Vehicle-to-Vehicle communications in highway platooning scenarios. *Ad Hoc Networks* 74, 17–29. doi:10.1016/j.adhoc.2018.03.004.
- Wang, M., 2018. Infrastructure assisted adaptive driving to stabilise heterogeneous vehicle strings. *Transportation Research Part C: Emerging Technologies* 91, 276–295.
- Wang, M., Hoogendoorn, S.P., Daamen, W., van Arem, B., Shyrokau, B., Happee, R., 2018a. Delay-compensating strategy to enhance string stability of adaptive cruise controlled vehicles. *Transportmetrica B* 6, 211–229. URL: <https://doi.org/10.1080/21680566.2016.1266973>, doi:10.1080/21680566.2016.1266973.
- Wang, P., He, X., Wei, Y., Wu, X., Wang, Y., 2022. Damping behavior analysis for connected automated vehicles with linear car following control. *Transportation research part C: emerging technologies* 138, 103617.
- Wang, Y., Xia, Y., Zhou, P., 2016. Fuzzy-model-based sampled-data control of chaotic systems: A fuzzy time-dependent lyapunov–krasovskii functional approach. *IEEE Transactions on fuzzy systems* 25, 1672–1684.
- Wang, Z., Bian, Y., Steven E. Shladover, 2019. A survey on cooperative longitudinal motion control of multiple connected and automated vehicles. *IEEE INTELLIGENT TRANSPORTATION SYSTEMS MAGAZINE* 12, 4–24. doi:10.3969/j.issn.1001-0505.2020.05.024.
- Wang, Z., Wu, G., Barth, M.J., 2018b. A review on cooperative adaptive cruise control (cacc) systems: Architectures, controls, and applications, in: 2018 21st International Conference on Intelligent Transportation Systems (ITSC), IEEE. pp. 2884–2891.
- Will, A.B., Z AK, S.H., 1997. Modelling and control of an automated vehicle. *Vehicle System Dynamics* 27, 131–155.
- Wilson, R.E., Ward, J.A., 2011. Car-following models: Fifty years of linear stability analysis - a mathematical perspective. *Transportation Planning and Technology* 34, 3–18. doi:10.1080/03081060.2011.530826.
- Wu, C., Li, Y., Li, Y., 2018. Trajectory tracking control for connected vehicle platoon considering time delays, in: 2018 Chinese Automation Congress (CAC), pp. 1328–1333. doi:10.1109/CAC.2018.8623721.
- Ye, L., Yamamoto, T., 2018. Impact of dedicated lanes for connected and autonomous vehicle on traffic flow throughput. *Physica A: Statistical Mechanics and its Applications* 512, 588–597.
- Yu, H., Jiang, R., He, Z., Zheng, Z., Li, L., Liu, R., Chen, X., 2021. Automated vehicle-involved traffic flow studies: A survey of assumptions, models, speculations, and perspectives. *Transportation research part C: emerging technologies* 127, 103101.
- Zhang, X., Jarrett, D.F., 1997. Stability analysis of the classical car-following model. *Transportation Research Part B: Methodological* 31, 441–462.
- Zheng, Y., Li, S.E., Wang, J., Cao, D., Li, K., 2015. Stability and scalability of homogeneous vehicular platoon: Study on the influence of information flow topologies. *IEEE Transactions on intelligent transportation systems* 17, 14–26.
- Zhong, Z., Lee, E.E., Nejad, M., Lee, J., 2020. Influence of CAV clustering strategies on mixed traffic flow characteristics: An analysis of vehicle trajectory data. *Transportation Research Part C: Emerging Technologies* 115, 102611.
- Zhou, L., Ruan, T., Ma, K., Dong, C., Wang, H., 2021. Impact of CAV platoon management on traffic flow considering degradation of control mode. *Physica A: Statistical Mechanics and its Applications* 581, 126193.
- Zhou, Y., Ahn, S., Wang, M., Hoogendoorn, S., 2020. Stabilizing mixed vehicular platoons with connected automated vehicles: An H-infinity approach. *Transportation Research Part B: Methodological* 132, 152–170.
- Zhou, Y., Wang, M., Ahn, S., 2019. Distributed model predictive control approach for cooperative car-following with guaranteed local and string stability. *Transportation research part B: methodological* 128, 69–86.
- Zhu, Y., He, H., Zhao, D., 2019. LMI-based synthesis of string-stable controller for cooperative adaptive cruise control. *IEEE Transactions on Intelligent Transportation Systems* 21, 4516–4525.